Wave Climate Projections off Coastal French Guiana based on High-Resolution Modelling over the Atlantic Ocean

Maurizio d'Anna, Léopold Vedie, Ali Belmadani, Déborah Idier, Rémi Thiéblemont, Philippe Palany, François Longueville

Ocean Modelling 194 (2025) 102468

Contents lists available at ScienceDirect

Ocean Modelling

journal homepage: www.elsevier.com/locate/ocemod

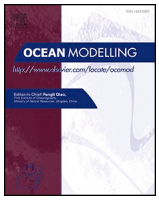

Wave climate projections off coastal French Guiana based on high-resolution modelling over the Atlantic Ocean

Maurizio D'Anna [a,*], Léopold Vedie [b], Ali Belmadani [c,d], Déborah Idier [e], Remi Thiéblemont [e], Philippe Palany [b], François Longueville [a]

[a] BRGM, 25 Av. Leonard de Vinci, 33600, Pessac, France
[b] Météo-France, Direction Interrégionale Antilles-Guyane, Fort-de-France, Martinique, France
[c] Météo-France, École Nationale de la Météorologie, Toulouse, France
[d] CNRM, Université de Toulouse, Météo-France, CNRS, Toulouse, France
[e] BRGM, 3 Av. Guillemin, 45060, Orléans, France

ARTICLE INFO

Keywords:
Climate change
Wave projections
Atlantic Ocean
French Guiana

ABSTRACT

Global warming is altering the atmosphere and ocean dynamics worldwide, including patterns in the generation and propagation of ocean waves, which are important drivers of coastal evolution, flood risk, and renewable energy. In French Guiana (northern South America), where most of the population is concentrated in coastal areas, understanding future wave climate change is critical for regional development, planning and adaptation purposes. The most energetic waves typically occur in boreal winter, in the form of long-distance swell originating from the mid-latitude North Atlantic Ocean. However, existing high-resolution wave climate projections that cover the French Guiana region focus on the hurricane season only (summer-fall). In this study, we used a state-of-the-art basin-scale spectral wave model and wind fields from a high-resolution atmospheric global climate model to simulate present and future winter (November to April) wave climate offshore of French Guiana. The model performance was evaluated against wave data from ERA5 reanalysis, satellite altimetry and coastal buoys between 1984 and 2013. For the future greenhouse gas emission scenario (Representative Concentration Pathway) RCP-8.5, we found a statistically significant overall projected decrease (~5 %) in wintertime average significant wave height and mean wave period, with a ~1° clockwise rotation of mean wave direction. The results suggest that these decreasing trends are primarily driven by changes in large-scale patterns across the Atlantic that counteract an expected increase in local wind speed. We discuss the implications of such projections for mud-bank dynamics along coastal French Guiana, although further local studies are required to address future coastal evolution and hazards. Finally, we identify a need for more in situ wave data near French Guiana to improve quantitative assessments of model performance and allow a correction of possible model biases.

1. Introduction

Climate change is altering the atmospheric circulation patterns that drive the generation and propagation of ocean waves (Reguero et al., 2019), and is expected to reshape global wave climate and associated extremes throughout the 21st century (Casas-Prat et al., 2024; Mark A. Hemer et al., 2013a; Lemos et al., 2021). Together with other hydrodynamic features, surface waves contribute to numerous coastal processes such as sediment transport, run-up and flooding (Toimil et al., 2020). Therefore, understanding the future evolution of wave climate is a key step for coastal management in the frame of climate adaptation (Cooley et al., 2022).

Located in the northern South America/equatorial Atlantic region, French Guiana hosts one of the most unique coastal systems on Earth. Embedded in the 1500-km long stretch of coast extending between the Amazon and Orinocco river mouths, it features dynamic mud banks formed by the Amazon River sediment discharge (Froidefond et al., 1988). These mud banks continuously interact with sandy beaches and rocky outcrops (Anthony et al., 2010; Jolivet et al., 2022), causing dynamic morphological and ecological changes on monthly to decadal time scales (Gensac et al., 2011; Wells and Kemp, 1986). Observations of the local shoreline evolution indicated that most of the erosion occurs

* Corresponding author.
E-mail address: maurizio.d.anna@upc.edu (M. D'Anna).

https://doi.org/10.1016/j.ocemod.2024.102468
Received 2 August 2024; Received in revised form 3 November 2024; Accepted 19 November 2024
Available online 28 November 2024

during the rain season (April-June) in response to northern swells and spring tide (Aertgeerts and Longueville, 2018; Longueville, 2017; Longueville and Lanson, 2022). Besides, the French Guiana coastal zone gathers ~90 % of the local population, as well as important assets such as the European Spatial Agency spaceport in Kourou, raising concerns about the exposure of the region to coastal hazards.

The complex morphodynamics of this coast is dominated by the alongshore migration of mud banks (Gardel and Gratiot, 2005), which is primarily controlled by ocean waves and currents (Gratiot et al., 2007). While recent studies have made significant progress in unravelling the inherent link between mud bank migration and incident waves (Abascal-Zorrilla et al., 2018, 2020; Gensac et al., 2015; Jolivet et al., 2019; Vantrepotte et al., 2013), future regional wave projections are essential in order to identify potential variations in the regime of mud bank dynamics and the cascading implications. As the local wave climate is strongly influenced by incoming swells from the North Atlantic Ocean, especially during the winter season (Anthony et al., 2011; Vantrepotte et al., 2013; Young, 1999), future wave projections offshore of French Guiana need to account for the effect of climate change over the entire Atlantic basin.

Over the last decade, much effort has been dedicated to projections of changes in mean and extreme wave conditions across the 21st century, on global scale (Camus et al., 2017; Casas-Prat et al., 2018; Fan et al., 2013, 2014; Mark A. Hemer et al., 2013a; Hemer et al., 2013a,b; Lemos et al., 2019; Lobeto et al., 2021, 2022; Meucci et al., 2020; Alberto 2024; Mori et al., 2010; Nobuhito 2013; Semedo et al., 2012; Alvaro 2013, 2018; Wang et al., 2014) and Atlantic basin scale (Belmadani et al., 2021; Bernardino et al., 2021; Cantet et al., 2021; D'Agostini et al., 2022; Webb et al., 2018). Many individual studies contributed to the Coordinated Ocean Wave Climate Project (COWCLIP, Hemer et al., 2018), forming a multi-model ensemble of global wave projections (Morim et al., 2020) forced by different Global Climate Models (GCMs) from the CMIP5 (Coupled Model Intercomparison Project, phase 5). This ensemble allowed mapping the spatially variable robustness (statistical significance) of the projected wave changes while analysing the uncertainties related to the use of different GCMs, wave models/statistical approaches and future greenhouse gas emission scenarios (Morim et al. 2019; Yadav et al. 2024). While most studies showed a consensus in modelled future trends over a large fraction of the Atlantic, the typical resolutions of GCMs (1–2°) and wave models (~1°) (Morim et al., 2020) result in hardly robust (not statistically significant) projections in tropical regions (Morim et al. 2019; Yadav et al. 2024). In the latter areas, modelling summertime tropical cyclones and the related waves requires finer resolutions of the forcing wind fields (Timmermans et al., 2017). However, during wintertime (DJF), when tropical cyclones are not expected, the COWCLIP ensemble shows yet a lack of robustness and large uncertainties (i.e., ensemble spread) (Morim et al., 2019). In the French Guiana area, the COWCLIP ensemble shows statistically significant change only in mean wave direction, and only at the north of the French territory's coastal area (Morim et al., 2019). Therefore, the COWCLIP projections in French Guiana as well as most of the tropical Atlantic region remain inconclusive, and more high-resolution studies are required to achieve robust wave projections in these areas.

Lately, updated GCMs with higher resolutions and improved physics have been developed within the more recent CMIP6 (Eyring et al., 2016), opening the way for a new generation of global wave projections (Alberto Meucci et al., 2024). Yet, these projections rely on ~1° resolution GCMs forcing wave models on a ~1° grid, and keep showing significant limitations in representing tropical wave climates (Meucci et al., 2023; Alberto 2024). Therefore, future trends in wave climate and extremes in the French Guiana region are still unclear.

Recently, Belmadani et al. (2021) derived future wave projections over the North Atlantic basin for the summer-fall (hurricane) season, focusing on changes in tropical cyclones and related wave extremes. They used wind fields from a global atmospheric GCM with a zoomed 0.15–0.25° grid over the North Atlantic to force a wave model covering the whole Atlantic basin at 0.5° resolution and including a nested 0.1° grid over the tropical North Atlantic band. Such fine resolutions allowed accounting for the influence of tropical cyclones on future wave climate, and producing statistically significant projections over most of the Atlantic basin. However, projections driven by high-resolution wind fields are still missing for the winter season, when French Guiana hydro- and morpho-dynamic coastal processes are most influenced by wave climate (Gratiot et al., 2007). In addition, while occurring typically during summer and fall, Atlantic tropical cyclones can also originate during the winter season (Collins and Roache, 2017), reinforcing the need for resolving wind fields at fine resolution. The current study aims at addressing future changes in mean and extreme wave conditions offshore of French Guiana for the winter season based on high-resolution wind fields, in order to inform future assessments of climate change impact on the local coastal processes. The current results will also complement existing summer season projections, advancing the state of the art of wave projections over the Atlantic Ocean. For this purpose, we use the high-resolution GCM winds (0.15–0.25°) and wave model (0.5°) adopted by Belmadani et al. (2021) over the Atlantic basin. The simulations are forced with a single GCM and consider a single scenario of future greenhouse gas emissions (Representative Concentration Pathway) RCP-8.5. We produced 5-member ensembles of multidecadal historical and future winter wave conditions over the Atlantic Ocean. The wave model performance offshore of French Guiana is evaluated against the ERA5 reanalysis, satellite altimetry and available coastal wave buoy data. We discuss the complementarity of the wave projections presented here with existing studies focused on the summer-fall season (Belmadani et al., 2021), leading to year-round state-of-the-art wave climate projections over the Atlantic Ocean, with particular focus on French Guiana. Finally, we discuss the annual and monthly COWCLIP multi-model projections near French Guiana to provide additional insights on future wave climate change in this area. While a full uncertainty assessment is hindered by the computational cost of such large-scale models, the current wave projections can provide a valuable contribution to future generations of high-resolution multi-model ensembles.

The remainder of the paper includes a description of the wind and wave data, the wave model and the methodology used herein (Section 2). The results of the model performance assessment and the wave projections are illustrated in Section 3 and discussed in Section 4. The conclusions of this work are drawn in Section 5.

2. Material and method

2.1. Wind data

Modelling the generation of ocean waves requires information on wind speed and direction near the sea surface. We used wind fields produced by Chauvin et al. (2020) who applied the very-high-resolution ARPEGE-Climat model, which is the atmospheric component of the CNRM-CM coupled GCM developed at Météo France.

Chauvin et al. run ARPEGE-Climat in the configuration adopted for CNRM-CM6 within the latest CMIP6 (Roehrig et al., 2020; Voldoire et al., 2019), but with a rotated and stretched spatial grid of 14km – 30km resolution over the tropical Atlantic region (Cantet et al., 2021). These settings allow the resolution of small-scale atmospheric patterns such as tropical cyclones (Chauvin et al., 2020), and small-scale details of the broader North Atlantic extratropical storms, ensuring that associated swells that may reach the coast of French Guiana are not overlooked.

ARPEGE-Climat was forced with monthly sea surface temperature (SST) fields obtained from the CMIP5 CNRM-CM5 model (Voldoire et al., 2013), for the historical period (1965–2013, hereon Hist-Model) and future (2031–2080) RCP-8.5 scenario. These prescribed SST fields were previously corrected using observed monthly SSTs (HadISST1, Rayner, 2003). Chauvin et al. (2020) also forced ARPEGE-Climat using

the observed HadISST1 SSTs directly, from 1965 to 2014, in an additional experiment (hereon Hist-Obs) for model comparison with observation data (Table 1).

Each experiment (Hist-Obs, Hist-Model and RCP-8.5) includes an ensemble of five model realizations (members) based on different initial conditions, i.e. forced with the same SST fields but exhibiting different chronologies of meteorological events. For instance, in the Hist-Obs experiment the five members were run with the same series of SSTs but with initial conditions (1st of January) corresponding to HadISST1 observations on the 1st of January of different years. For each experiment and respective ensemble members, ARPEGE-Climat simulations provide 6-hourly fields of 10-m wind vectors interpolated over a 0.5° regular grid.

The reader is referred to Chauvin et al. (2020) for further details on the climate model and the associated simulations. For our applications, we extracted wind data from the latest modelled 29 winter seasons (November – April) for each experiment and ensemble member proposed by Chauvin et al. (2020), i.e. Hist-Obs, Hist-Model and RCP-8.5 (Table 1).

Over the historical period, the ARPEGE-Climat wintertime (NDJFMA) mean wind speed 10 m above the sea surface (U_{10}) reaches its largest values in the tropical band (roughly along the 15°N parallel) and decreases towards French Guiana. This pattern represents typical winter conditions, characterized by stronger trade winds and the Intertropical Convergence Zone located closer to the equator (Fig. 1a) compared to summer (Fig. 3a of Belmadani et al., 2021). In the RCP-8.5 future scenario, ARPEGE-Climat projects a slight intensification of the northeasterly trade winds, with a statistically significant increase in mean U_{10} near northern South America, including the French Guiana region (Fig. 1b). In addition, over the southeastern area offshore of French Guiana, the wind field undergoes a mild counter-clockwise rotation (Figure S1). In the mid-latitudes (30–50°N) of the Atlantic basin, changes are rather heterogeneous, although the projections show a statistically significant overall reduction of winter mean U_{10} in this region (Fig. 1b). The projected changes and the respective statistical significance are estimated using the method presented in Section 2.4.3.

2.2. Wave data

Data of past offshore wave conditions is fundamental to evaluate the wave model performance, and support the interpretation of wave projections with the associated uncertainties in the French Guiana region.

Table 1
Summary of ARPEGE-Climat simulations including: SST forcing and experiments; time slices modelled by Chauvin et al. (2020) and used in the present study; number of model realizations.

ARPEGE-Climat model experiment	Forcing monthly SST	Simulated time slice	Extracted data	# ensemble members
Hist-Obs	HadISST1	1965–2014	November 1985-April 1986 to November 2013-April 2014 (hereafter 1985–2013)	5
Hist-Model	CNRM-CM5, historical, corrected with HadISST1	1965–2013	November 1984-April 1985 to November 2012-April 2013 (hereafter 1984–2012)	5
RCP-8.5	CNRM-CM5, RCP8.5, corrected with HadISST1	2031–2080	November 2051-April 2052 to November 2079-April 2080 (hereafter 2051–2079)	5

The following sections introduce the available data used for model comparison over the historical period (Hist-Obs).

2.2.1. ERA5 reanalysis

ERA5 (Hersbach et al., 2020) is a high-resolution (31 km grid cell size, regridded data available at 0.5° resolution) hourly reanalysis of global atmospheric, land surface and ocean surface variables produced by the European Centre for Medium-Range Weather Forecasts (ECMWF) within the Copernicus Climate Change Services. The reanalysis is based on a rich set of globally distributed data from modelling and observation starting from 1940, and includes the reconstruction of hourly wave conditions obtained from an atmospheric model coupled with the European Centre Wave Action Model (ECWAM). For the model comparison, we extracted ERA5 estimates of significant wave height (H_s), mean wave period (T_m) and mean wave direction (D_m) from 1985 to 2013.

Global estimates of historical wave hindcasts and reanalyses such as ERA5 are affected by uncertainties due to different calibration data and modelling approaches (Erikson et al., 2022; Kodaira et al., 2023; Morim et al., 2022, 2023). In particular, ERA5 has been shown to underestimate wave heights in the North Atlantic region (Dodet et al., 2020; Hawkins et al., 2022; Kodaira et al., 2023; Timmermans et al., 2020) and, like most historical datasets (excluding wave buoys), is not expected to provide accurate estimates in coastal areas, where complex nearshore processes are not resolved by such global models. However, during the winter season, most available datasets show consistent trends over most of the Atlantic Ocean (Erikson et al., 2022). For these reasons, we conducted complementary comparisons of the historical model runs (Hist-Obs) against the observed satellite and coastal wave buoy data (Section 2.2.2).

2.2.2. Wave buoys and satellite data

Four wave buoys were deployed in different locations off the coast of French Guiana, with data records available from the *Centre d'Archivage National de Données de Houle In Situ* (CANDHIS). For the comparison with historical wave simulations (Sections 3.1 and 2.4.2), we used two of these buoys located at ~20 km offshore of Cayenne (97,304) and Kourou (97,303), both at 20 m depth (Figs. 2a,b). Data from the two remaining buoys are excluded as they are likely affected by local coastal processes (Text S1 of Supplementary Material).

Figs. 2c,d show the yearly and monthly distributions of 30-min wave records available from these two buoys during winter. The temporal coverage of the datasets is limited (Fig. 2c) to one winter for the 97,303 buoy and two winters for the 97,304 buoy, with multiple gaps (Fig. 2d).

Wave observations off the coasts of French Guiana are also available from satellite altimetry. The European Space Agency Climate Change Initiative (ESA-CCI) level 4 multi-mission product version 1.1 (Dodet et al., 2020; Piollé et al., 2020) provides monthly mean H_s with a 1° (~110 km) resolution. ESA-CCI data also include monthly exceedance probabilities of H_s for the 1 m, 1.5 m, 2 m and 3 m threshold values. Along the coastal band, the mean and extreme H_s estimates should be interpreted carefully, as they may be contaminated by the influence of land and wave form retrievals. We note that satellite data are associated with uncertainties due to e.g. atmospheric corrections and sampling frequency, and are only available from 1991, limiting the comparison with the Hist-Obs results to the 1991–2013 23-year period. While the satellite data cover a shorter period than ERA5, they are derived from observations and are not affected by the limitations of numerical modelling. In addition, a 23-year record remains sufficient for an assessment of model performances. On the other hand, while buoy records provide in situ direct information that is not affected by biases associated with modelling (e.g. reanalysis) and processing (e.g. satellite altimetry), they are limited to very localised areas and cover short periods of time. Therefore, the complementary strengths of the three data sources (ERA5, ESA-CCI, CANDHIS) provides more confidence in the interpretation of the model performance over the historical period.

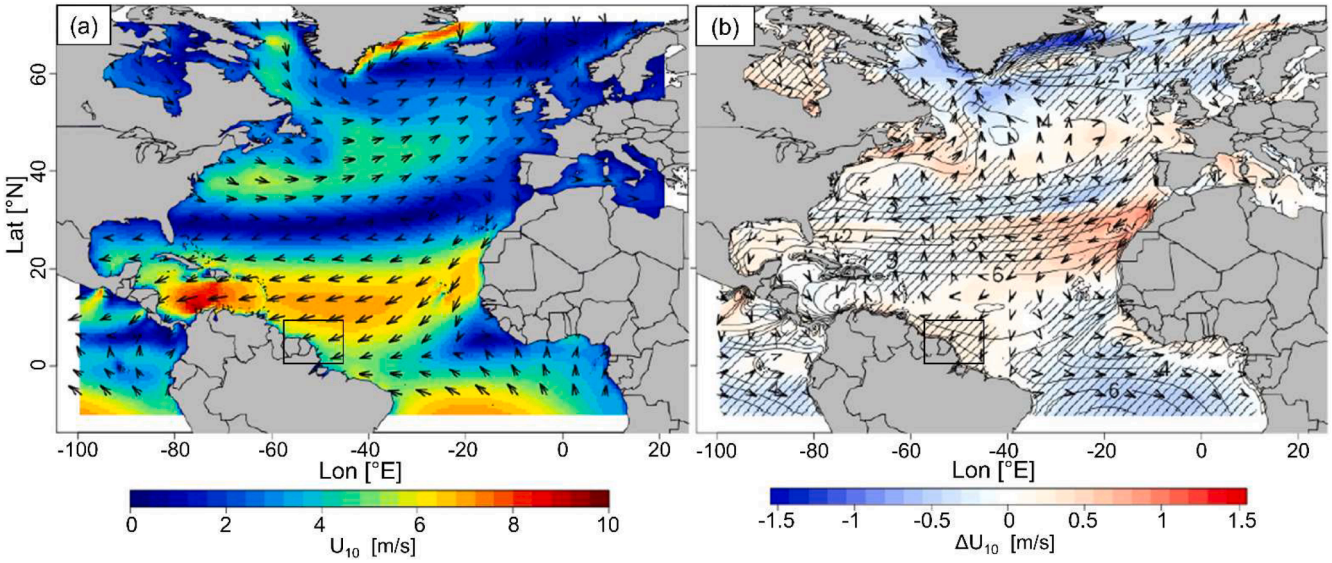

Fig. 1. Mean present-climate NDJFMA surface wind speed U_{10} (shading, m s^{-1}) and direction (arrows) for the (a) Hist-Obs (1985–2013) experiment, and respective changes (ΔU_{10} shading, m s^{-1} and directional arrows) for the (b) future RCP-8.5 (2051–2080) scenario. Hatchings indicate statistically significant changes based on Student's *t*-test and FDR control (see Section 2.4.3). Black boxes indicate the region considered for the French Guiana regional analyses (see Section 2.4.1).

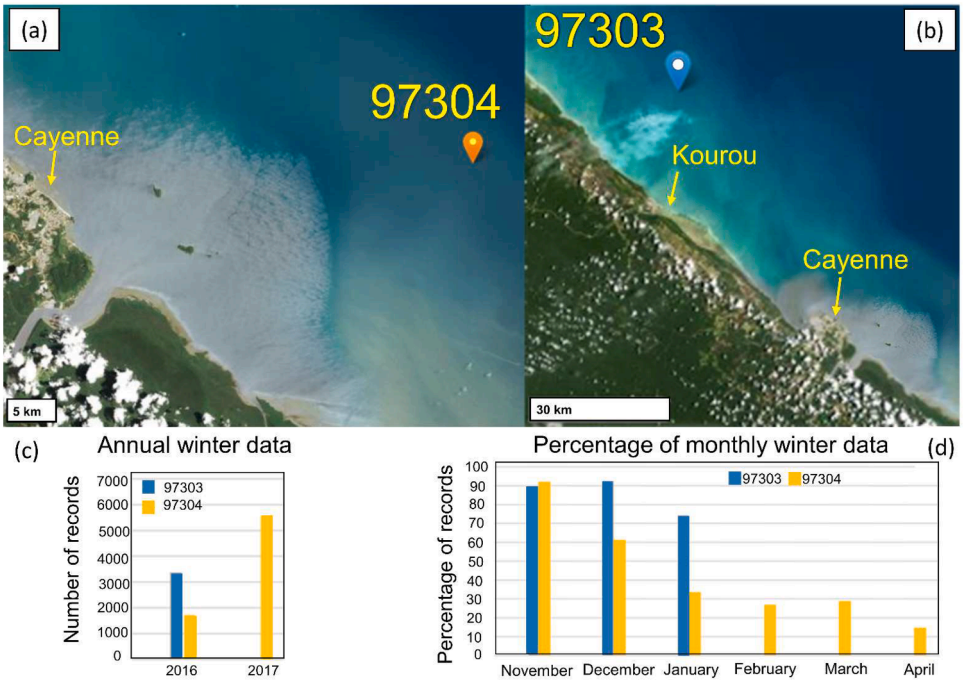

Fig. 2. Locations of wave buoys in French Guiana's coastal region, offshore of (a) Cayenne (97,304) and (a) Kourou (97,303) (source: https://candhis.cerema.fr/_public_/cartes.php), and the respective (c) annual number of semi-hourly records during winter (NDJFMA) and (d) monthly percentage of available winter data.

2.3. Wave model

We modelled past and future wave conditions offshore of French Guiana using the MFWAM (Météo-France Wave Action Model), an operational third-generation spectral wave model. MFWAM was developed by Météo-France on the basis of WAM (WAMDI-Group, 1988), which is widely used for global and regional modelling studies including future projections that contributed to the COWCLIP ensemble (e.g. Semedo et al., 2018).

The model simulates the generation and propagation of wave energy in response to forcing wind fields by resolving the spectral energy balance, adopting the dissipation term proposed by Ardhuin et al. (2010) and updated by the Copernicus Marine Service. MFWAM also has a similar configuration of ECWAM used to produce ERA5 data. The modelled spectra are discretized into 24 directions (15° interval) and 30 frequencies ranging from 0.035Hz to 0.58Hz. MFWAM is forced with 2-D 10-m wind time series, produces 3-hourly values of H_s, T_m and D_m, and has been extensively validated against wave buoy data, showing among the best forecasting skill across the Atlantic Ocean (Bidlot, 2017).

Here, we run MFWAM in the configuration adopted by Belmadani et al. (2021), where the model domain covers most of the North and South Atlantic basins (59.5°S to 70°N) with a 0.5° grid (MFWAM05). We note here that Belmadani et al. (2021) also used a nested 0.1° grid (MFWAM01) focusing on the main development region of tropical

cyclones. As the finer domain (MFWAM01) southern boundary runs close to the coast of French Guiana, here we used the MFWAM05 grid alone. A 0.5° resolution is sufficient to accurately model the propagation of swell waves across the Atlantic basin, and is of the order of the highest resolutions adopted by existing state-of-the-art global wave models (Morim et al., 2020). In addition, previous MFWAM applications suggested that, despite the higher resolution of the wind forcing, an increased (0.5° to 0.1°) grid resolution did not have a significant impact on the model results in deep waters, except for a weak sensitivity of extreme wave conditions (Belmadani et al., 2021).

2.4. Method

2.4.1. Wave model setup

For the wave model applications, we forced winter wave simulations with the ARPEGE-Climat 6-hourly wind fields obtained from the five members of the three climate experiments introduced in Section 2.1 (Hist-Obs, Hist-Model and RCP-8.5). The use of five-member ensembles for each experiment allows accounting for the uncertainties related to the inherent variability of the climate circulation (Mankin et al., 2020), and increases the robustness of the model results, especially for extreme events (Belmadani et al., 2021; Meucci et al., 2020; Timmermans et al., 2017). Given the computational burden of multiple MFWAM simulations and the study focus on the winter season, we modelled wave conditions (H_s, T_m, D_m) from 1st November to 30th April (NDJFMA) for 29 following years, for each experiment ensemble. This resulted in 435 time series (3-hourly) of winter wave conditions (Table 2).

We run the historical simulations of wave conditions over the period 1985–2013 and 1984–2012 for the Hist-Obs and Hist-Model experiments, respectively. The former is compared against historical wave data to assess the model accuracy, and the latter is compared to the RCP-8.5 projections to quantify future changes in modelled wave climate. Herein, we analyse and discuss the possible bias in model results against available data as described in Sections 2.4.2, 3.1 and 4.1, although bias correction (e.g. Charles et al., 2012) is not performed (see Section 4.1). The future scenario (RCP-8.5) is run from 2051 to 2079, which corresponds to the latest 29 years of available wind fields from the climate model experience (Section 2.1).

In order to analyze wave climate change offshore of French Guiana, we extracted the MFWAM results over the portion of the domain included between (59.5° - 48° W) and (2° - 12° N), hereafter referred as MFWAM05* (Fig. 3). As we aim at characterizing the change of deep-water waves, this area extends several hundreds of kilometres offshore of French Guiana's coasts to ensure deep water conditions of the modelled waves. For the analysis of the seasonality of modelled wave conditions (Section 2.4.3), the results are spatially integrated over a part of MFWAM05* excluding nearshore areas (red region in Fig. 3), where waves are strongly affected by complex processes that are not resolved by MFWAM (Anthony et al., 2010). For each experiment, an average 2-D wave field is derived by averaging the results obtained from the five respective ensemble members.

Table 2
Summary of the MFWAM simulations including: 6-hourly wind forcing experiments, simulated winter period and time slices, and number of model realizations.

MFWAM model experiment	Simulated time slice	Winter period simulated each year	# ensemble members	Total # simulations
Hist-Obs	1985–2013	November 01 – April 30	5	145
Hist-Model	1984–2012	November 01 – April 30	5	145
RCP-8.5	2051–2079	November 01 – April 30	5	145

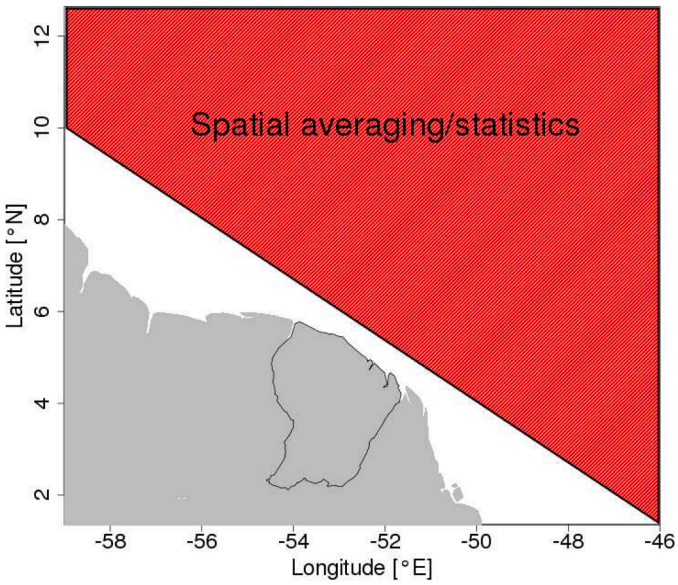

Fig. 3. Portion of the MFWAM model domain considered for the analysis over the French Guiana region (MFWAM05*), with a sub-portion (red-shaded area) excluding the coastal band, used to calculate spatial averages and other statistics for the analysis of mean seasonal cycles of modelled wave variables.

2.4.2. Model bias assessment

When addressing future wave climate, it is fundamental to investigate possible biases in model results for a proper interpretation of the projections, especially beyond decadal scale (Bitner-Gregersen et al., 2022; Khandekar, 1989; Lemos et al., 2020). Therefore, as a preliminary step, we compared the wave model results of the Hist-Obs simulation with the available historical data from ERA5, ESA-CCI and wave buoys (Section 2.2).

We remind here that while the MFWAM Hist-Obs simulations are forced with wind data obtained from observed SST fields, each ensemble member is based on different initial conditions and does not ensure a consistent chronology with the observations. This does not allow the quantification of performance metrics derived from the direct comparison of time series (e.g. root-mean-square-error).

First, we compared H_s and T_m winter mean ($\overline{H_s^w}$, $\overline{T_m^w}$) and 95th percentile ($H_{s,95}^w$, $T_{m,95}^w$) obtained from the Hist-Obs simulation with ERA5 data over the period 1985–2013 within the MFWAM05* domain. Then, we interpolated the Hist-Obs results to match the grid of ESA-CCI data and compared the mean and extreme H_s for the winter season. In this case, extreme H_s are expressed as monthly exceedance probabilities of four threshold values 1 m, 1.5 m, 2 m, and 3 m, which correspond to the values provided by ESA-CCI (Piollé et al., 2020). Finally, a pointwise analysis is performed for the winter season between the wave buoy data and the Hist-Obs results extracted at the nearest grid points ([52°W; 5°N] for 97,304 i.e. 6 km away, and [52.5°W; 5.5°N] for 97,303 i.e. 20 km away). For this comparison, the wave buoy data and 3-hourly model results are represented using box-plots indicating the 25th, 50th and 75th percentiles for H_s and T_m, and using wave roses for D_m.

Ultimately, we also compared the Hist-Obs and Hist-Model simulations to verify the consistency between the two historical ensembles (Section 3.1).

2.4.3. Projected winter wave changes

In order to investigate winter wave climate change between the 1984–2012 and 2051–2079 periods in the French Guiana region, we analysed the differences between the RCP-8.5 and Hist-Model ensembles by mapping the evolution of winter wave characteristics (mean H_s and T_m, i.e. $\overline{H_s^w}$ and $\overline{T_m^w}$, and median D_m, i.e. $D_{m,50}^w$) and the respective statistical robustness. The latter is evaluated applying statistical

significance tests with control of the False Discovery Rate (FDR) (Benjamini and Hochberg, 1995), which adjusts the resulting *p-values*. The calculation of *p-values* requires the statistical independence of the analysed variables, which we obtained applying a temporal subsampling of the wave data through the computation of decorrelation maps, following the approach proposed by Belmadani et al. (2021) (see Text S2 of Supplementary Material). Finally, the *p-values* are estimated at each model grid point using a Student, Welch or Wilcoxon test based on the probability distribution and variance of the tested variable (Figure S5 of Supplementary Material). This methodology is also applied to the RCP-8.5 and Hist-Model winter U_{10} fields (Fig. 1b) to analyse the projected winter wave climate in light of future changes in the wind forcing. We performed the procedure with the 3-hourly H_s and T_m, and the 6-hourly U_{10} subsampled every 5 days and 10 days, respectively.

The average of instantaneous wave directions ($\overline{D_m^w}$) does not correspond to the mean wave direction D_m extracted from the winter mean directional wave spectrum and is not necessarily representative of typical wintertime values, introducing potential biases. Compared to $\overline{D_m^w}$, the median represents the more frequent D_m and is less susceptible to biases. Thus, we evaluated the evolution of mean wave direction (rotation) by observing its winter median value ($D_{m,50}^w$) at each grid point across the MFWAM05* domain. The analysis of directional wave roses at five locations off the French Guiana coast for the Hist-Model and RCP-8.5 experiments suggests that the median represents the real wave rose well, i.e. the wave directions are distributed smoothly (near Gaussian) and do not show multiple peaks that may bias the representativeness of the median (Text S3 of Supplementary Material). Herein, a negative (positive) change in $D_{m,50}^w$ represents clockwise (counterclockwise) rotation.

Extremes of the 3-hourly winter wave characteristics are represented here by the respective 10-year return values, obtained from Generalized Extreme Value (GEV) distributions of the annual maxima of the 145 simulated winter seasons for Hist-Model and RCP-8.5. The significance of the estimated changes in extreme values is assessed based on the 95 % confidence bounds (2.5th - 97.5th percentiles) of the return values (Belmadani et al., 2021) obtained with a bootsrapping of annual maxima (1000 iterations with replacement) and the respective GEVs.

We also estimated the RCP-8.5 return period corresponding to the 10-year Hist-Model return values in order to identify possible increases/decreases in the occurrence frequency of historical 10-year extreme events (Wang et al., 2014).

Further, we analysed the seasonal variability of the projected wave climate by computing the climatological daily means of H_s, T_m and $H_s^2T_m$, spatially averaged over the portion of MFWAM05* excluding nearshore areas (red area in Fig. 3). Herein, we consider $H_s^2T_m$ to synthesize the wave energy (E). For each calendar date of the winter season (NDJFMA), we estimated the mean of the 145 (5×29) values from all the simulated members and years, obtaining an average seasonal cycle of the different variables over the selected area, for the Hist-Model and RCP-8.5 experiments. Then, we applied a 30-day running average to filter out the isolated storm events occurring on intra-monthly time scales.

The seasonal variability of extreme H_s, T_m and $H_s^2T_m$ is assessed in a similar fashion as the climatological daily mean values, extracting the spatial maxima over the same portion of MFWAM05* (red area in Fig. 3) at each time step and selecting the daily maximum. This results in 145 values of spatial maxima for each calendar day of the winter season. Then, we evaluate the associated climatological daily exceedance probability, defined as the daily fraction of values (within the sample of 145 values) exceeding a prescribed threshold. We defined the latter threshold by testing several values and retained those that resulted in realistic probability curves, i.e. characterized by a relatively smooth temporal distribution (not too noisy between consecutive days) and a realistic occurrence probability (rare enough for the events to qualify as extremes). Finally, we smoothed the seasonal cycles applying a 30-day running mean.

3. Results

The MFWAM model produced 3-hourly series of H_s, T_m and D_m throughout the winter season (1st November to 30th April) for 29-year periods under three experiments (Hist-Obs, Hist-Model and RCP-8.5), each one including five ensemble members. The following subsections illustrate the comparison between modelled wave conditions and available data over the historical period 1985–2013 (Section 3.1), as well as the MFWAM winter wave changes projected for 2051–2079 (Section 3.2).

3.1. Model performance

The comparison between Hist-Obs results and ERA5 (Section 2.2.1), wave buoys and ESA-CCI data (Section 2.2.2) provides an indication of the MFWAM model performance in representing mean and extreme historical winter wave conditions over the 1985–2013 period. Fig. 4 shows the differences between Hist-Obs and ERA5 fields of wintertime mean and 95th percentile H_s (Fig. 4a,b) and T_m (Fig. 4c,d) over the MFWAM05* domain, and the ERA5 reference values (black contours). The ERA5 $\overline{H_s^w}$ and $\overline{T_m^w}$ fields reach 2.2 m and 8.0 s, respectively, and both decrease from the northeastern end of the domain to the French Guiana coasts (Fig. 4a,c). A similar pattern is observed for $H_{s,95}^w$ and $T_{m,95}^w$, which decrease from 3 m and 10 s to 2–2.5 m and ~9 s (Fig. 4b,d). Hist-Obs produces a northeast to southwest decrease in $\overline{H_s^w}$ and $\overline{T_m^w}$ consistent with ERA5 data (not shown). The model results show an overall underestimation of $\overline{H_s^w}$ (~0.15 m, i.e. ~10 %, on average), with well represented extremes showing a mild overestimation of 0.1–0.2 m (5–7 %) and underestimation of ~0.1 m (~5 %) in the northwestern and southeastern areas of the domain, respectively (Fig. 4a,b). In contrast, the model generally overestimates T_m over the domain with biases of the order of 0.5–0.8 s (5–10 %) for the winter mean values and 10–15 % for the extremes (Fig. 4c,d).

Compared to ESA-CCI data, the Hist-Obs $\overline{H_s^w}$ shows a larger bias than the one observed against ERA5, with an overall underestimation of 0.3–0.4 m (20–30 %) (Fig. 5a). The results show a smaller bias and $\overline{H_s^w}$ overestimation in the coastal areas north and south from French Guiana, although both ESA-CCI and MFWAM data are highly uncertain in nearshore zones (as stated in Section 2). The probability of H_s exceeding 2 m or 3 m (extreme waves) is consistent between Hist-Obs and ESA-CCI, with a decay in the occurrence of H_s>2 m and H_s> 3 m as waves approach the continent (Fig. 5b, 5c). However, Hist-Obs results in a slightly more gradual decay (milder gradients) than ESA-CCI 2- and 3- m exceedance probability across the MFWAM05* domain (Fig. 5b,c). Such difference is also observed for lower thresholds of exceedance (1 m and 1.5 m), as shown in Figure S7 of Supplementary Material.

The analysis of MFWAM performance is complemented by comparing the Hist-Obs results with in situ data from coastal wave buoys (Section 2.2.2). The 97,304 buoy data and the nearest model results ([52°W; 5°N]) show nearly matching values of the median winter H_s ($H_{s,50}^w$~1.32–1.33 m), though with a narrower confidence interval for the model results, which overestimate and underestimate the 25th and 75th percentiles, respectively, by ~8 % (Fig. 6a,b). In respect to the 97,303 buoy, located in the vicinity of Kourou (Fig. 2a), the nearest model predictions ([52.5°W; 5.5°N]) overestimate the median winter H_s ($H_{s,50}^w$~1.39 m vs 1.22 m) and the 25th percentile ($H_{s,25}^w$~1.16 m vs 1.02 m) by ~14 %, and underestimates the 75th percentile ($H_{s,75}^w$~1.66 m vs 1.72 m) by ~3 % (Fig. 6c,d). The 25th and 75th percentiles, and median values of T_m are very consistent with differences of 1–2 % off Cayenne (Fig. 6c,d) and <1 % off Kourou (Fig. 6c,d). The agreement with winter wave data from the buoys provides a good validation of the model, considering that the Hist-Obs climate simulations are forced with

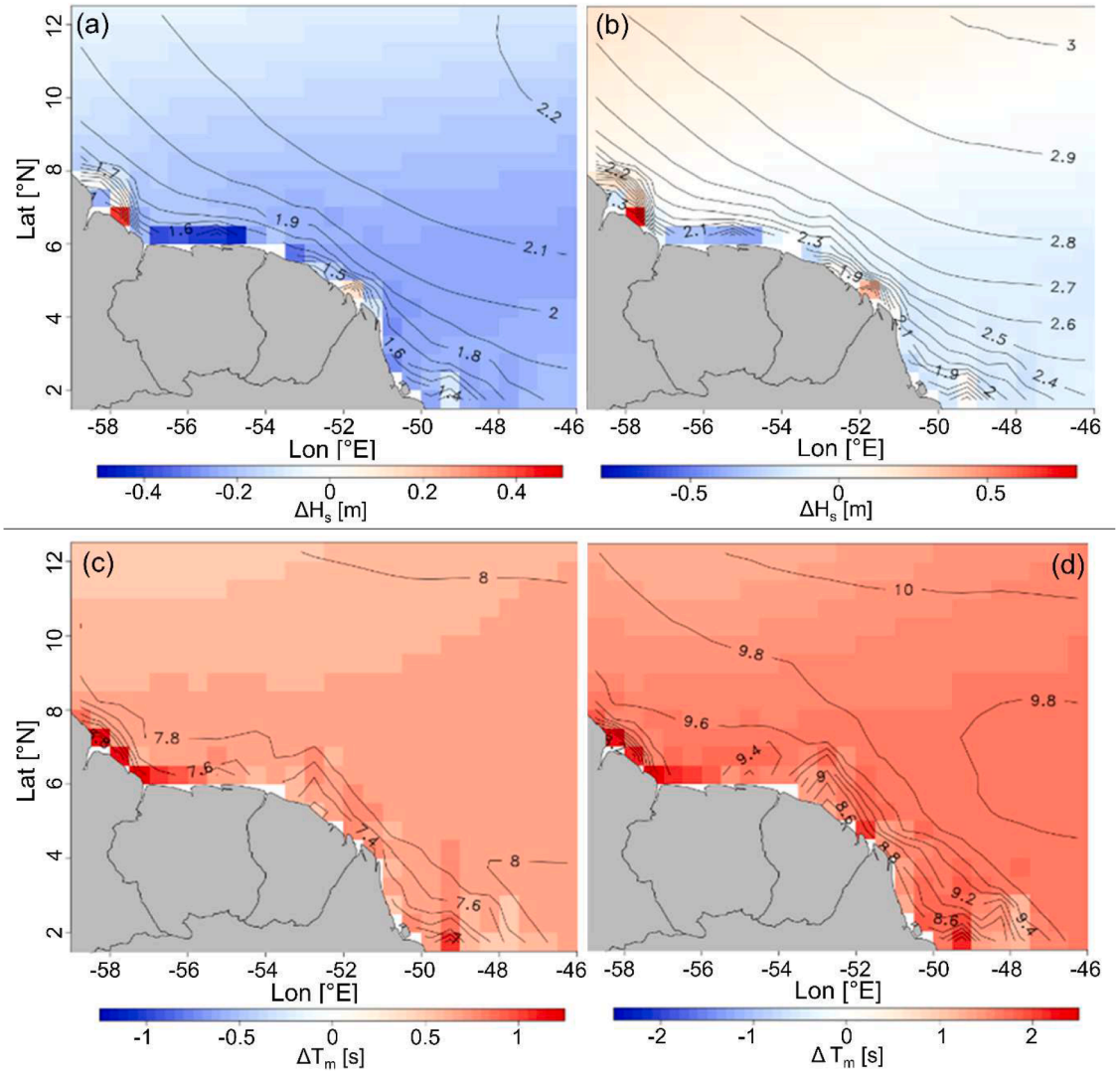

Fig. 4. Comparison between Hist-Obs and ERA5 winter wave conditions (Hist-Obs minus ERA5) over the 1985–2013 period, including changes in: (a) winter mean H_s ($\Delta\overline{H_s^w}$); (b) 95th percentile H_s ($\Delta H_{s,95}^w$); (c) winter mean T_m ($\Delta\overline{T_m^w}$); and (d) 95th percentile T_m ($\Delta T_{m,95}^w$). Black isocontours indicate the reference ERA5 values.

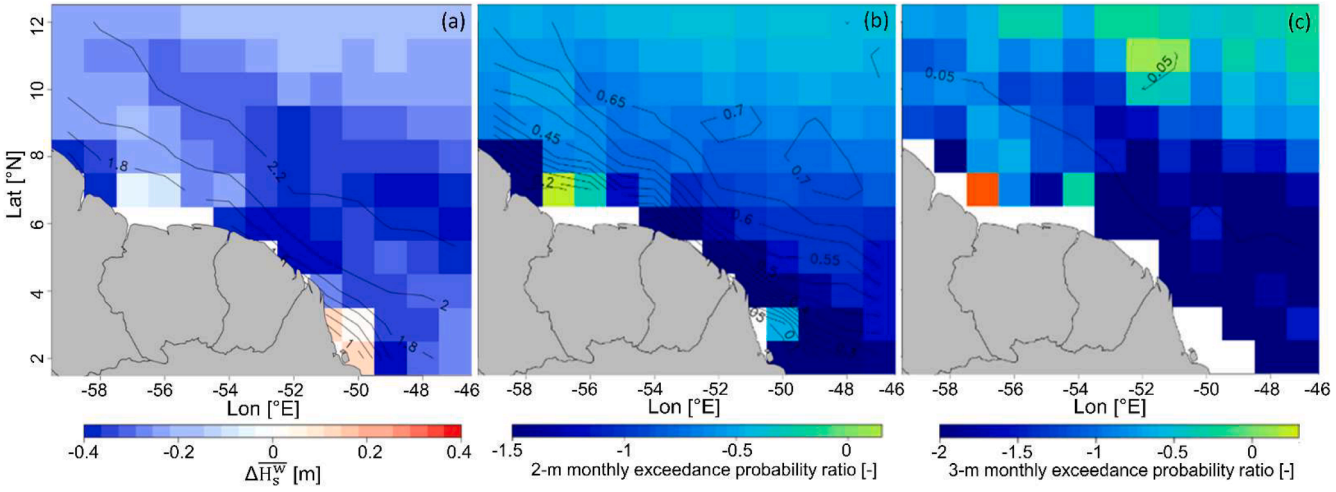

Fig. 5. Comparison between Hist-Obs and ESA-CCI winter wave conditions over the 1991–2013 period, including differences in: (a) winter mean H_s ($\Delta\overline{H_s^w}$, Hist-Obs minus ESA-CCI); (b) 2-m and (c) 3-m monthly exceedance probability, expressed as the ratio (Hist-Obs/ESA-CCI) of probabilities on a power (base 2) scale, i.e. −0.05 corresponds to $2^{-0.05}$ ~0.966. Black isocontours indicate the reference ESA-CCI (a) $\overline{H_s^w}$ values and (b) probabilities.

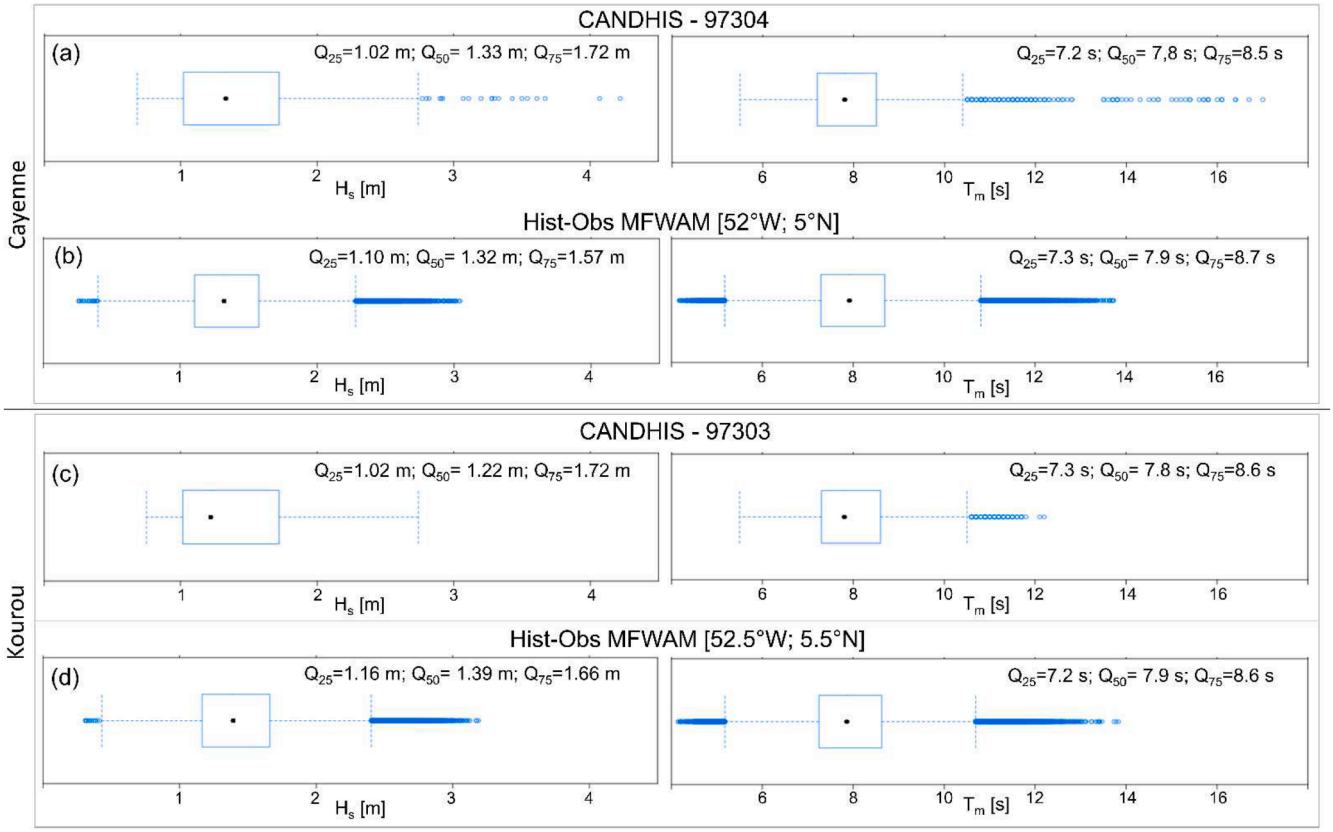

Fig. 6. Box plots (25th, 50th and 75th percentiles) of H_s and T_m from (a) the CANDHIS 97,304 buoy and (b) Hist-Obs [52°W; 5°N] MFWAM grid point near Cayenne; and (c) the CANDHIS 97,303 buoy and (d) Hist-Obs [52.5°W; 5.5°N] MFWAM grid point near Kourou.

observed monthly SSTs without any data assimilation in the wave model or its wind forcing.

The wave roses representing the buoy records offshore of Cayenne (97,304) and Kourou (97,303) both show an incident direction of winter waves primarily from the NE (>50 %) and NNE (~35 %) sectors, with most of the largest waves ($H_s > 2$ m) coming from the NE sector (Fig. 7a, c). Consistently, the modelled winter waves and their extremes at the two nearest grid points mainly come from the NE (>60 %). On the other hand, in both locations, less than 20 % of modelled waves come from the NNE sector and include only waves up to 1.8 m (Fig. 7b,d). Offshore of Cayenne, this difference is mostly compensated by more waves falling into the NE sector, while near Kourou it is evenly distributed in the neighbour directional sectors (NNE and ENE) (Fig. 7b,d). Both buoys also recorded ~10 % of waves (up to 1.8 m) coming from the N sector, which do not appear in the model results. Hence, both comparisons offshore Cayenne and Kourou suggest a mild clockwise bias of the model.

The Hist-Obs and Hist-Model results over the 1985–2012 period show notable differences mainly in the mid-high latitudes, corresponding to a westward shift of winter mean and extreme H_s in the Hist-Obs experiment (Figures S8 of Supplementary Material). However, in the tropical latitudes and French Guiana region the two experiments reproduce the same overall wintertime wave climate (Figure S9 of Supplementary Material), consistently with the outcomes of Chauvin et al. (2020) and the summertime comparison performed by Belmadani et al. (2021) over the Atlantic Ocean.

Overall, despite some biases between the Hist-Obs experiment and the three reference datasets, and recalling the uncertainties and limitations affecting reanalysis, satellite and buoy data, it is concluded that the model reproduces fairly well the winter wave climate in the study area over the historical period. This, together with the agreement between the Hist-Obs and Hist-Model experiments (Section 2.4.2), confirms the MFWAM suitability to evaluate future changes in winter wave climate offshore of French Guiana.

3.2. Winter wave projections

The future wave projections from RCP-8.5 (2051–2079) and the historical wave conditions from Hist-Model (1984–2012) are used to derive projected changes of the winter wave climate off the coasts of French Guiana in the RCP-8.5 scenario. Fig. 8a,b show that the model predicts a statistically significant reduction (3–5 %) of $\overline{H_s^w}$ and $\overline{T_m^w}$ over the whole study area (MFWAM05*) by 2051–2079. The projected changes in mean $\overline{H_s^w}$ ($\overline{T_m^w}$) are larger in the northern (coastal) area of the domain, and gradually decrease towards (away from) the French Guiana coast (Fig. 8a,b). The modelled historical (Hist-Model) winter waves show a rather homogeneous spatial pattern of $D_{m,50}^w$ (black arrows in Fig. 8c), characterized by median direction mostly from the NE, turning towards ENE in the northwest area of the domain and NNE in the southeast. Fig. 8c also shows an overall projected clockwise rotation between 1° and 3° of winter wave angle, with larger changes in the northwestern area of the domain and smaller changes in the southeast, accentuating the spatial variability of $D_{m,50}^w$. The examination of wave roses extracted from the RCP-8.5 and Hist-Model results at five locations confirm that the median of D_m well represents the actual incident wave direction offshore of French Guiana (Text S3 of Supplementary Material).

For the Hist-Model experiment, the 10-year return values of H_s (T_m) vary between 3 m (13.5 s) a few tens of kilometres off the coast, and >4.2 m (>15.5 s) in the northern area of the domain as shown in Fig. 9a (Fig. 9b). The historical extreme values of E show similar contours as H_s, with magnitudes ranging between 50 m^2s and 250 m^2s (Fig. 9c). The simulated future winter wave climate (RCP-8.5) shows an overall 5 %

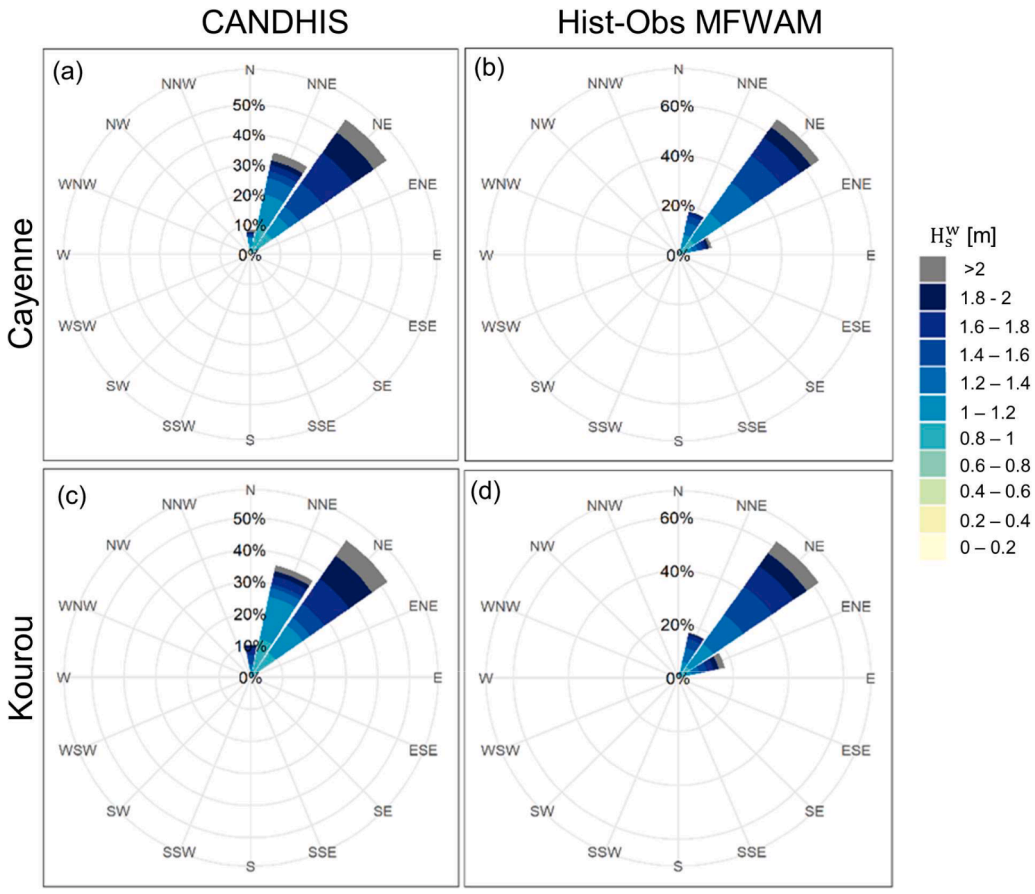

Fig. 7. Wave roses of winter conditions offshore of: Cayenne from (a) the 97,304 wave buoy, and (b) Hist-Obs [52°W; 5°N]; and Kourou from (c) the 97,303 wave buoy and (d) Hist-Obs [52.5°W; 5.5°N], with colour scale indicating different ranges of winter H_s.

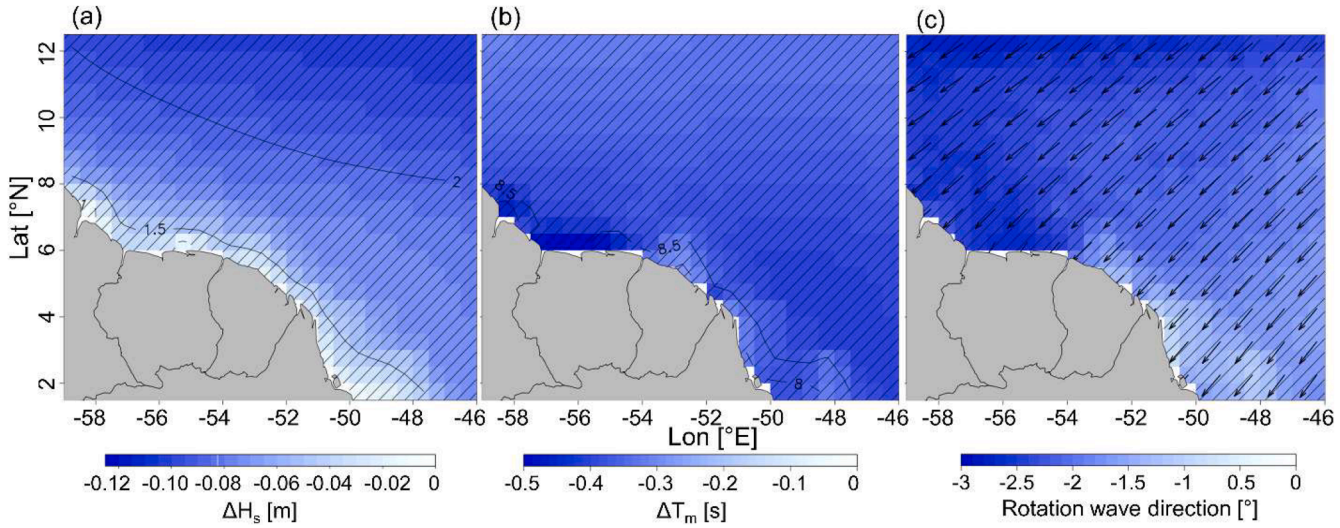

Fig. 8. Projected changes in winter mean wave climate (2051–2079) for the RCP-8.5 scenario relative to Hist-Model historical conditions (1984–2012), including: (a) $\Delta\overline{H_s^w}$ and (b) $\Delta\overline{T_m^w}$ with black contours indicating the reference Hist-Model values and hatchings indicating statistically significant changes (using p-values and control of False Discovery Rate, Section 2.4.3); and (c) $\Delta D_{m,50}^w$ with arrows indicating the reference Hist-Model wave directional pattern. Negative $\Delta D_{m,50}^w$ indicate clockwise rotation.

decrease in 10-year return H_s, which is stronger and statistically significant in the northwestern to central area of the domain (7–8 %) and smaller near the coasts and in the southeastern part of the domain (3–4 %, Fig. 9a). For the extreme T_m, the projections show a small increase (1–2 %) in the northeast, and a decrease of the order of 3–4 % towards the coasts, although these changes are statistically significant only in over a small part of the southeastern coastal region (Fig. 9b). An overall decrease of ~10 % in the derived extreme E is projected, with changes statistically significant in the central portion of the domain (where projected change reach 15 %) and in isolated coastal areas off French

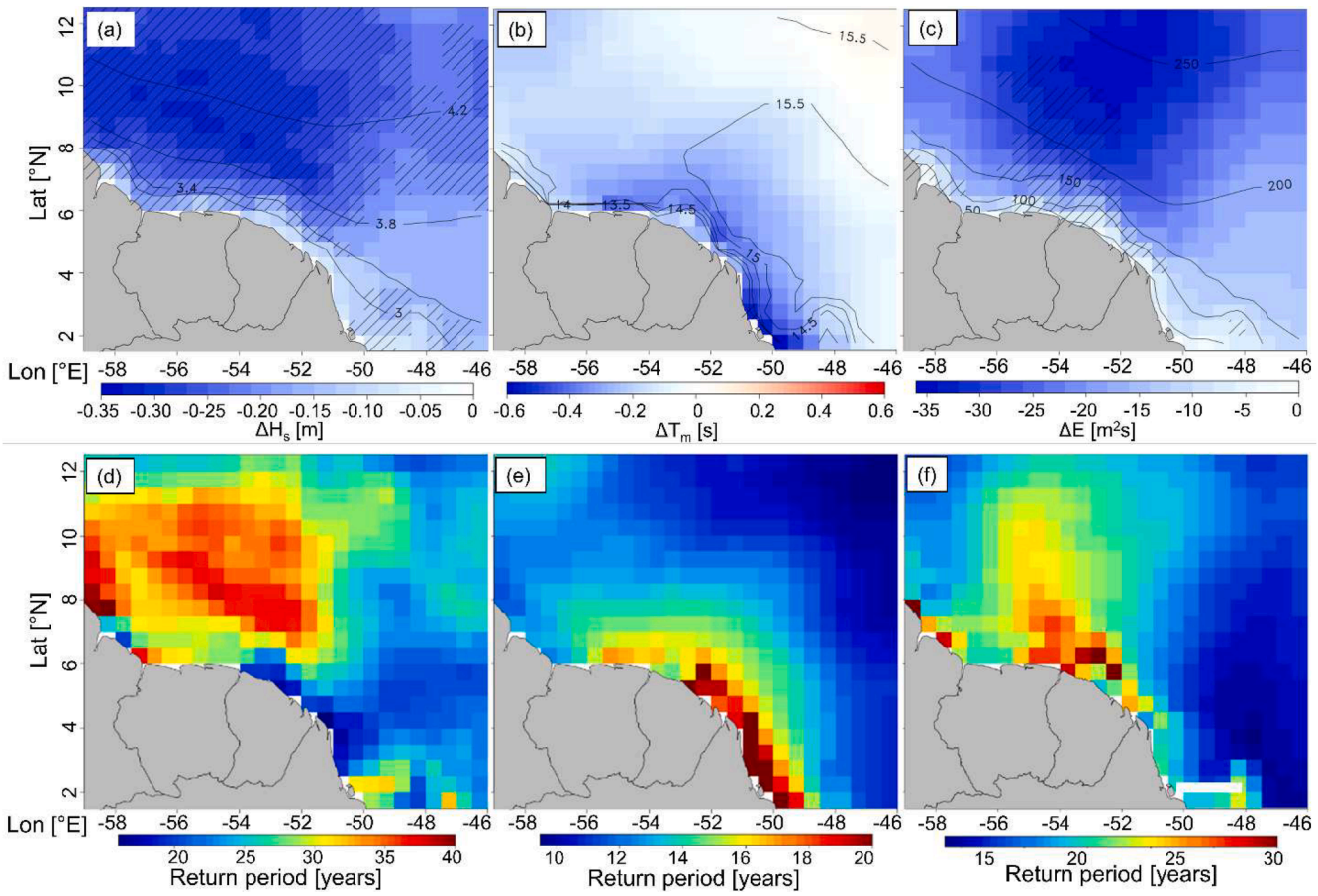

Fig. 9. Projected changes in (a-c) 1 in 10 years winter waves for the RCP-8.5 (2051–2079) scenario relative to Hist-Model historical (1984–2012) conditions, illustrating the evolution of extreme values for: (a) H_s, (b) T_m and (c) $E = H_s^2 T_m$; and (d-f) future RCP-8.5 return periods (years) corresponding to the Hist-Model (1984–20,123) 10-year return (d) H_s, (e) T_m, and (f) E. Black contours indicating the reference Hist-Model values and hatchings indicating statistically significant changes (using p-values and control of False Discovery Rate, Section 2.4.3).

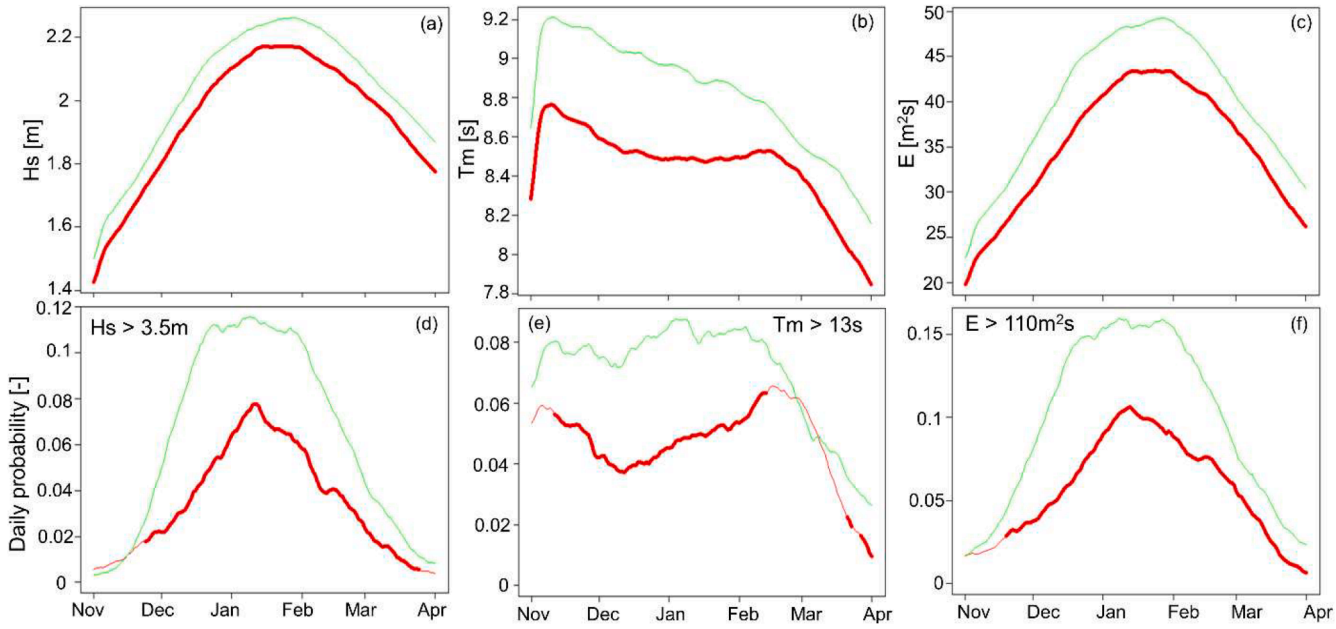

Fig. 10. Seasonal variability (in winter) of climatological daily mean (a) H_s, (b), T_m, and (c) $H_s^2 T_m$, and daily probability of exceeding (d) 3.5 m for H_s, (e), 13 s for T_m, and (f) 110 m^2s for $H_s^2 T_m$, including Hist-Model historical (green curves) and projected RCP-8.5 data (red curves). Bold red lines indicate statistically significant ($p < 5$ %) projected changes.

Guiana (Fig. 9c). Fig. 9d-f shows the RCP-8.5 projected return periods corresponding to the Hist-Model 10-year return values for H_s, T_m and E. For H_s, the historical 10-year return values are projected to be associated with a return period ranging from 15 years at the French Guiana coast, up to 35–40 years in the western part of the domain (Fig. 9d). The future return periods for the historical decadal T_m values gradually increase from the northeastern end of the region (~10 years) to the coasts (~20 years, Fig. 9e). For wave energy, future return periods grow up to 15–25 years, peaking in the central-western part of the domain (Fig. 9f).

Fig. 10 shows the seasonal variability of historical and projected mean wave characteristics and the respective exceedance probabilities within the winter season (NDJFMA). Between November and February, the historical climatological daily mean H_s and $H_s^2T_m$ gradually increase from 1.5 m to 2.2 m and from 25 m^2s to 50 m^2s, respectively, and then decrease to H_s=1.9 m and $H_s^2T_m$=30 m^2s by April (Fig. 10a,c). In contrast, in the beginning of the season, the daily mean T_m undergoes a rapid growth (within a few days) from 8.6 s to 9.2 s, followed by a gradual decrease to 8.8 s by March, and an accelerated decrease to 8.2 s by April (Fig. 9b). Fig. 9a,b indicates that the statistically significant decrease observed for $\overline{H_s^w}$ and $\overline{T_m^w}$ (Fig. 8a,b) persists evenly throughout the winter season. Consequently, the daily mean energy (E) exhibits a similar trend, although with enhanced projected decrease at the season peak, in January-February (Fig. 9c).

Fig. 10d-f illustrates the probabilities that the climatological wintertime daily maxima of historical and future modelled H_s, T_m and E exceed 3.5 m, 13 s, and 110 m^2s, respectively. All the analyzed variables exhibit an overall reduction of exceedance probability of the respective thresholds, which is consistent with the projected changes observed for the 10-year return values (Fig. 9). The projected probabilities for H_s and E are the highest in the second half of January compared to the longer period (early January to mid-February) observed in the Hist-Model experiment, with a ~30 % decrease for both parameters (Fig. 10d,f). The peak occurrence probability of future T_m extremes decreases by 35–40 % (from ~0.08 to ~0.05) and remains stable between November and February, as per the historical simulation, although with a predicted drop in December-January (Fig. 10e).

4. Discussion

4.1. Model performance

The Hist-Obs results over the French Guiana region showed a general underestimation of the winter mean significant wave height compared to ERA5 reanalysis and ESA-CCI satellite data (Section 3.1). Moreover, the model shows larger differences against ESA-CCI data (20–30 %) than against ERA5 (~10 %). This appears consistent with the tendency of ERA5 reanalysis to underestimate H_s observations in the North Atlantic basin (Hawkins et al., 2022; Timmermans et al., 2020), although ESA-CCI data is also affected by uncertainties due to the sampling frequency and data processing.

In a recent assessment of global wave model skill against ERA5 wave data, the 1979–2004 average H_s from two wave models forced with CMIP6 GCMs exhibited mild positive biases (<10 % overestimation) in the French Guiana region (Meucci et al., 2023). Interestingly though, over the 1985–2014 period, one of the models (forced with the EC-Earth GCM) showed a statistically significant decreasing trend in annual mean H_s near French Guiana, in contrast to the ERA5 statistically significant increasing trend, both larger than 1.75 %/decade (Fig. 12 of Meucci et al., 2023). Consequently, over the 1985–2014 period, this wave model tends to increasingly underestimate the ERA5 annual mean H_s data offshore of French Guiana, supporting the findings of our comparison for the wintertime season (Section 3.1). The second CMIP6-driven model (forced with the ACCESS-CM2 GCM) also produced a decreasing H_s trend in the French Guiana region, although not statistically significant.

MFWAM performs better in reproducing extreme H_s, with biases generally <7 %. The source of this bias may be attributed (at least partially) to the surface wind speed (U_{10}) produced by ARPEGE-Climat, which underestimates the ERA5 data both in the tropics (by up to 1.5 m/s off French Guiana) and north of 50°N (by up to 2–2.5 m/s) (see Fig. 1a and S9). In addition, the model reproduces very well the mean H_s conditions measured by the wave buoys offshore of Cayenne and Kourou, with much weaker negative biases.

MFWAM also proved to have good skills in reproducing the wintertime mean wave period, with excellent performances relative to wave buoy data, and a relatively small bias against ERA5 estimates (10–15 % overestimation). In terms of median D_m, the model features a systematic, though small, clockwise rotation compared to the buoy wave roses. While the latter bias may be partly related to a corresponding bias in the forcing wind fields, which show a slight clockwise difference against ERA5 winds (Figure S11b of Supplementary Material), the origins of the mild biases in T_m is not straightforward.

Overall, despite the presence of some biases, the model performs well over the historical period, thus supporting the application of MFWAM for the simulation of future winter wave climate. However, further assessment of the model performance and the application of bias correction methods to the wave projections require the development of long uninterrupted wave data from measurements or extensively validated hindcasts (e.g. Charles et al., 2012).

4.2. Wave climate change

4.2.1. Projected winter wave changes

The MFWAM RCP-8.5 experiment results predict an overall negative trend in winter mean H_s and T_m as well as a slight clockwise rotation of $D_{m,50}^w$ in the French Guiana region by the 2051–2079 period. This appears to be in contrast with the projected intensification of wind speed and the counter-clockwise rotation of the northeasterly trade winds (Section 2.1). However, the general decrease observed for $\overline{H_s^w}$ and $\overline{T_m^w}$ in the French Guiana region can be explained by the larger-scale signal of modelled wave conditions. In fact, an analysis of the model results over the North Atlantic basin reveals a basin-wide reduction, the strongest decrease in $\overline{H_s^w}$ occurring around 60°N and 30–40°N, thereby reducing the historical gradients between the larger mid-latitude waves and the smaller tropical waves (Fig. 11a). Such $\overline{H_s^w}$ changes are most likely linked to an overall weakening of the mid-latitude future winds (Fig. 1b) and to those weather types (synoptic patterns) that associate weaker storms along the mid-to-high latitudes, which are projected to become more frequent during winter (Lemos et al., 2021).

As North Atlantic swells are the dominant component of sea states approaching the French Guiana coasts in the winter season (Anthony et al., 2011; Young, 1999), the weakening of such swells may be identified as the main driver of projected changes in $\overline{H_s^w}$ offshore of French Guiana compared to wind sea. However, the increase in wind speed projected for the RCP-8.5 scenario over the tropical band (Fig. 1b) may contribute to the attenuation of $\Delta\overline{H_s^w}$ (decrease) equatorward from 30°N (Fig. 11a). In contrast, the modelled changes in $\overline{T_m^w}$ are more pronounced south of 30°N, near the west-African and South-American coasts, including the French Guiana region (Fig. 11b). The stronger reduction in $\overline{T_m^w}$ over the latter area is located on the edge of the signal observed for the main changes in $\overline{H_s^w}$, suggesting that these two variables are linked by the southwards propagation of North Atlantic swells. Indeed, if North Atlantic swells are reduced in the future, the wave dispersion in deep water will drive a decrease in $\overline{T_m^w}$ that intensifies with distance from the source.

The trends featured in our winter projections between 1984 and 2012 and 2051–2079 in the French Guiana region are consistent with the COWCLIP winter projections between 1979 and 2004 and 2080–2099, with $\overline{H_s^w}$, $\overline{T_m^w}$ and $D_{m,50}^w$ changes falling in the respective

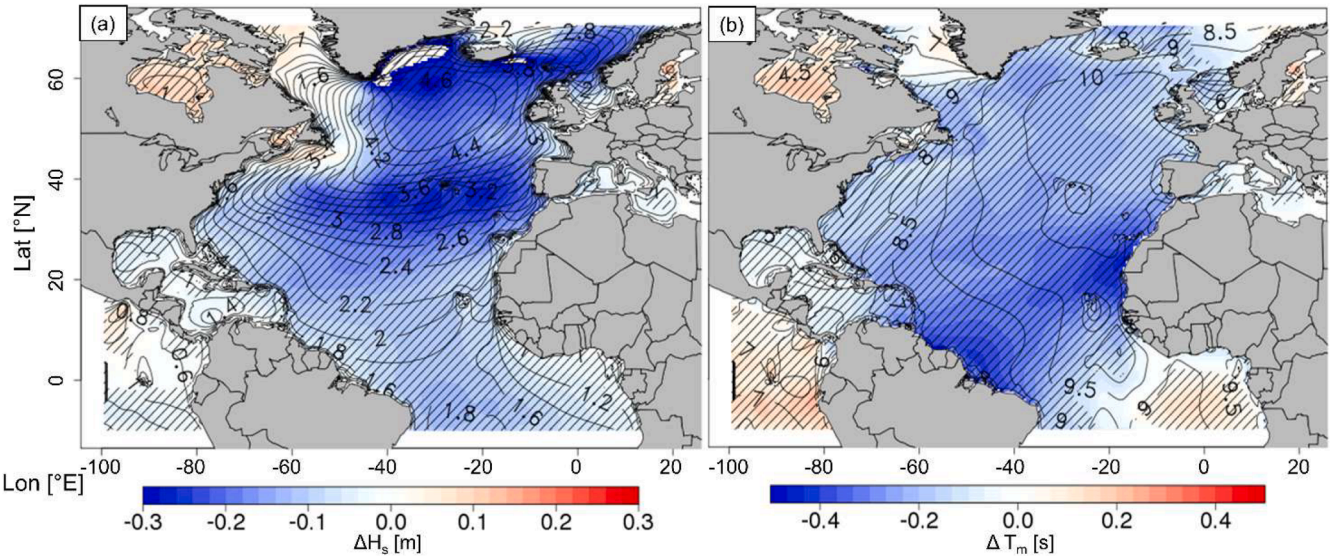

Fig. 11. Projected changes in winter mean wave climate for the RCP-8.5 scenario (2051–2079) relative to Hist-Model historical conditions (1984–2012) over the North Atlantic basin: (a) $\Delta\overline{H_s^w}$ and (b) $\Delta\overline{T_m^w}$, with black contours indicating the reference Hist-Model values and hatchings indicating statistically significant changes.

ranges of values predicted by the multi-model ensemble (Section 4.2.3).

The analysis of 10-year return values for wave height, period and energy suggests that current winter extremes will occur more rarely in the future (Fig. 9), and will be more concentrated around the month of January (Fig. 10). Indeed, the historical (Hist-Model) 10-year events are projected to associate return periods between 15 and 40 years in the future (RCP-8.5). This is in line with existing global projections, which predicted an overall annual decrease in 20-year (Lobeto et al., 2021) and 100-year (Meucci et al., 2020) return H_s by the end of the 21st century for the RCP8.5 scenario in the North Atlantic basin. While the results of the latter studies are associated with low statistical significance near French Guiana (Lobeto et al., 2021; Meucci et al., 2020), the statistical significance of our projections provide more confidence to the predicted trends. However, our projected extremes may still present some uncertainties, e.g. stemming from the uncertainties affecting future extratropical storm tracks (Lobeto et al., 2021; Meucci et al., 2020).

4.2.2. Seasonality of wave climate change

Our winter wave projections are complementary to Belmadani et al. (2021)'s projections of summer-fall wave climate (hurricane season) over the Atlantic basin, which are based on the same modelling framework. The summer-fall season simulations (Fig. 5b,c of Belmadani et al. 2021) showed a statistically significant decrease in seasonal mean H_s over the French Guiana region, and in seasonal mean T_m near French Guiana's coast (and non-statistically-significant increase offshore), both at rates similar to the ones obtained from our winter projections, resulting from changes in large-scale patterns. The latter lead to an overall mean reduction of 5–10 % in H_s and ~5 % in T_m throughout most of the year near French Guiana coast. We note here that the summer-fall (July - November) and winter (November - April) projections do not include the May - June period. On a larger scale, this is in line with the outcomes of previous studies, which obtained the same order of decrease in annual mean H_s by 2100 over the North Atlantic region for the RCP-8.5 scenario (Bricheno and Wolf, 2018; Charles et al., 2012). Similar trends, though with different intensities (0–7 % decrease), were observed also by Meucci et al. (2023) across the Atlantic Ocean for a similar greenhouse gas concentration scenario.

Similarly to our modelled changes of 10-years return winter wave events (Fig. 9), Belmadani et al. (2021) also projected a decrease in extremes during the summer-fall season over the Atlantic Equatorial region by 2051–2080, though of lower magnitude and statistically significant only near the coast. The Authors attributed this change to a poleward migration of extreme wave heights in response to the associated summertime tropical cyclone activity. Instead, the decrease of 10-years H_s projected near French Guiana during the winter season is mostly driven by a decrease in extreme wind-wave significant height (H_{s0}) over the mid- and high-latitudes (20°N-30°N), and the consequent decrease in significant height of primary swells (H_{s1}) coming from the North (Figure S10 of Supplementary Material).

4.2.3. COWCLIP multi-model projections

The COWCLIP projections indicate a statistically significant clockwise change in annual mean D_m of ~1° in the northern coastal area of French Guiana (*Figure 3* of Morim et al., 2019), which is in line with the MFWAM results for the wintertime season (Section 3.2). Further north, along the Surinam coast, COWCLIP also predicts a statistically significant decrease in annual mean T_m (*Figure 3* of Morim et al., 2019), which, given the relatively coarse resolutions of the ensemble members, may extend to the French Guiana region. This is consistent with the combined MFWAM summertime and wintertime projections offshore of French Guiana (Section 4.2.2).

We further investigate the annual and monthly averages of COWCLIP wave projections at the interpolated grid point (see Text S4 of Supplementary Material) closest to the French Guiana coast (52°W; 6°N) for the RCP4.5 and RCP8.5 scenarios. This allowed a qualitative comparison with the MFWAM winter projections, and the investigation of the marginal (scenario-based) uncertainties associated with future greenhouse gas emissions, as well as uncertainties in climate model and wave modelling approach (Morim et al., 2019). The projected changes in H_s, T_m and D_m are estimated as the difference of the respective annual and monthly averages between 2081 and 2099 and 1979–2004, for each available climate-wave model combination of the ensemble (Table S1 of Supplementary Material). It is worth noting that, unlike our analysis, COWCLIP considers the changes in mean D_m and not its median value. For each ensemble of projections (and for both annual and monthly means), we estimate the 95 % confidence interval (2.5th - 97.5th percentiles) of the ensemble mean by applying an empirical bootstrapping method (1000 iterations).

The multi-model ensemble predicts larger changes in wave characteristics for the RCP8.5 scenario compared to RCP4.5 for both annual and monthly means (Fig. 12), suggesting that the respective uncertainties are mostly driven by the combination of GCM and wave model. This corroborates the findings of Morim et al. (2019)'s investigation of the relative contributions of uncertainties in RCP scenario,

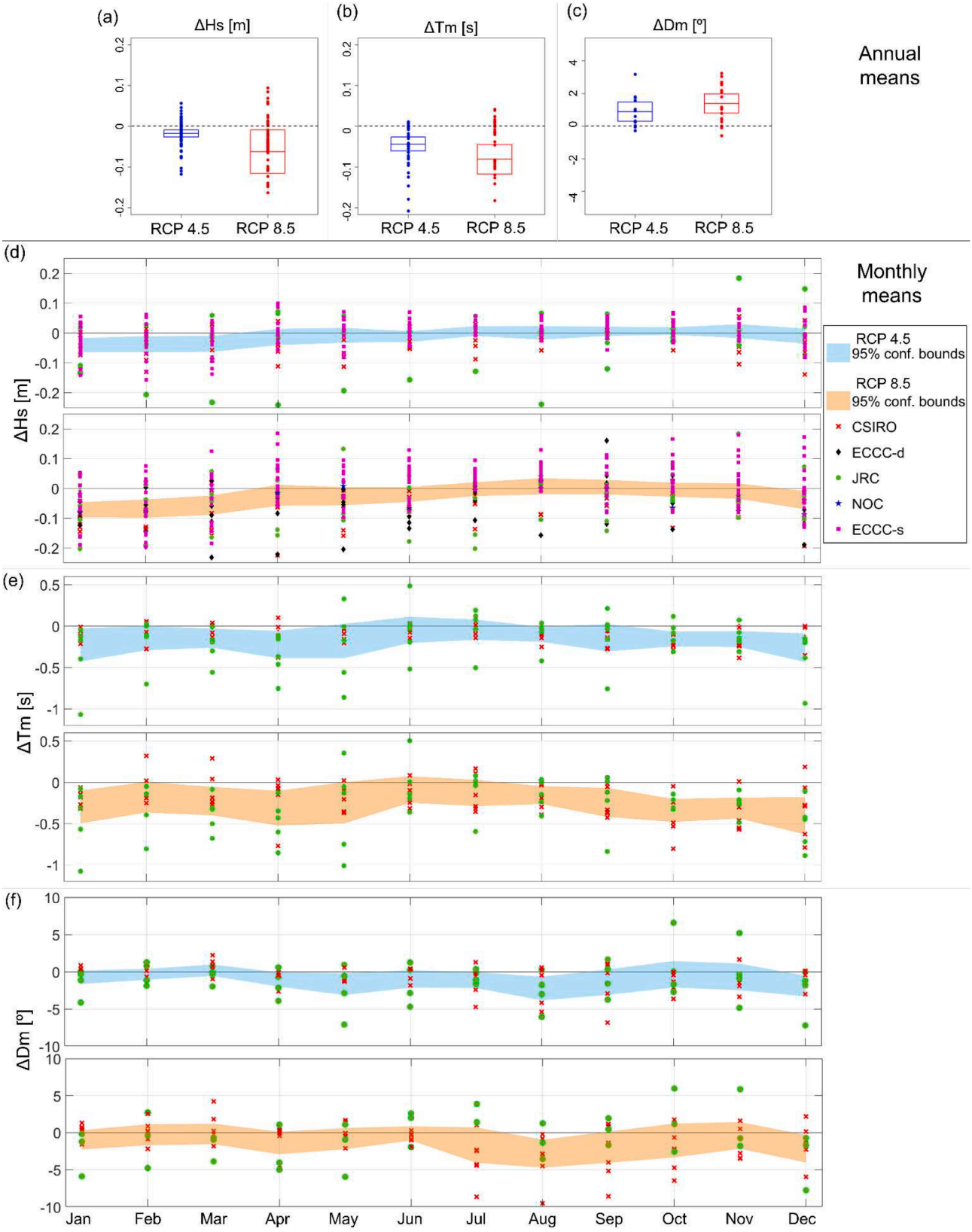

Fig. 12. COWCLIP 2081–2099 ensemble projections relative to 1979–2004, including projected changes in annual (a-c) and monthly means (d-f) of (a,d) H_s, (b,e) T_m and (c,f) D_m, for the RCP4.5 (blue) and RCP8.5 (red) scenarios, extracted at the nearest grid point to French Guiana (52°W; 6°N). Box-plots (a-c) indicate the 25th, 50th and 75th percentiles of the ensemble projections. Shaded areas indicate the 95 % confidence intervals of ensemble mean values.

GCM and wave model (including their interactions), to the COWCLIP projection total uncertainties (Morim et al., 2019).

The monthly changes show an overall reduction in H_s and T_m, with stronger changes from December to April (winter) for both RCP4.5 and RCP8.5 scenarios, while the monthly mean D_m is predicted to rotate clockwise throughout the year (Fig. 12d-f). Although the monthly changes in H_s and T_m remain negative across the respective confidence intervals between December and March, some ensemble members yet predict opposite trends (positive) over this period (Fig. 12d,e). Meanwhile, the monthly confidence interval of projected D_m always includes positive (counter-clockwise) values of modelled rotation, although with a strong asymmetry towards negative (clockwise) values (Fig. 12f). Hence, an increase in H_s and T_m, and/or a counter-clockwise rotation of D_m cannot be excluded, undermining the robustness of the COWCLIP projections at this location and confirming (Morim et al., 2019) results.

Nonetheless, while uncertain, the COWCLIP projections are in line with the MFWAM projections discussed herein (Sections 4.2.1 and 4.2.2), providing a qualitative validation of our projected trends. Indeed, despite the different time slices being considered, for the RCP8.5 scenario the wintertime (NDJFMA) ensemble mean COWCLIP projected changes in H_s, T_m and D_m are of the order of -3 %, -4 % and $\sim 1^\circ$ clockwise, respectively, against -3–5 %, -3–5 % and 1–3° clockwise for MFWAM.

The choice between a dynamic or statistical downscaling approach does not seem to have a significant impact on the uncertainties (ensemble confidence interval) for the changes in monthly mean H_s (Text S4 of Supplementary Material). In fact, Fig. 12d shows that the statistically downscaled members (ECCC-s) are well distributed within the range of modelled results in the winter months.

4.3. Implications for coastal French Guiana

The projected changes in future wave climate may affect the evolution and migration of mud banks, which control the morphodynamics of the French Guiana coast. As mud-bank dynamics respond to the wave-driven longshore currents (Eisma et al., 1991; Lakhan and Pepper, 1997), the expected clockwise rotation of wave direction may reduce the northeast component of the incident power, altering the rates of bank migration. In addition, the largest effects of waves on mud occur during high-energy events that follow extended low-energy periods (Gratiot et al., 2007). Hence, despite the projected decrease in $\overline{H_s^w}$ and $\overline{T_m^w}$, the narrowed period of likely winter extremes in H_s and in wave energy (more concentrated in January, Fig. 10d,f) results in longer calm periods preceding high-energy events, which may lead to increased suspension of sediment from the mud banks. On the other hand, the general decrease in $\overline{H_s^w}$ of North Atlantic swells (Fig. 11a) will likely reduce the resuspension of sediments (Vantrepotte et al., 2013). However, the future evolution of mud-bank dynamics along the coasts of French Guiana also depends on changes in the Amazon River sediment supply and in tidal currents (Anthony et al., 2010; Froidefond et al., 1988; Gardel and Gratiot, 2005). Therefore, the effects of wave climate change on the dynamics of French Guiana mud banks are not straightforward and require further investigation of the concurrent action of waves and other drivers (Vantrepotte et al., 2013).

In terms of coastal hazard, future sea-level rise is already expected to trigger or increase chronic flooding in tropical regions (Le Cozannet et al., 2021), including French Guiana (Longueville et al., 2022; Thiéblemont et al., 2023). Our analysis of future wave climate evolution suggests that the sole effect of waves should not exacerbate flood hazard (assuming no significant impact on mud bank migration), and that considering an unchanged wave climate is a conservative assumption for coastal flood hazard assessment in French Guiana (Longueville et al., 2022). However, neglecting the impact of wave climate change on the migration of mud banks, which can behave as flood defence, is a strong assumption. Therefore, a detailed assessment of future flood hazard in French Guiana requires more local studies accounting for the influence of wave climate change on mud-bank migration.

4.4. Assumptions and limitations

Wave modelling is affected by uncertainties related to model calibration, forcing conditions, and parametrization of some physical processes. Such uncertainties can cascade through the assessment of important processes, e.g. future shoreline evolution (D'Anna et al., 2022; Toimil et al., 2021) and coastal flooding (Parodi et al., 2020; Vousdoukas et al., 2018), and affect the support of decision making for coastal adaptation to climate change (Hinkel et al., 2019, 2021). Although based on 5-member ensembles, the projections presented here are based on a single combination of wave model and GCM, which does not allow the quantification and analysis of uncertainties. However, our winter projections may be integrated in future ensemble-based seasonal assessments of wave climate change, or combined with existing summertime projections and complementary May-June projections (Section 4.2.2) for annual assessments over the Atlantic Ocean, in a similar fashion to the COWCLIP ensemble (Morim et al., 2019).

The wave projections presented here did not undergo any model bias correction. The application of bias correction methods, such as *quantile-quantile* corrections (Déqué, 2007) is becoming a common practice in the context of wave climate modelling (Casas-Prat et al., 2024; Charles et al., 2012; Lemos et al., 2020; Gil 2024; Lira Loarca et al., 2023), and can help reducing the uncertainties in future projections, including those for extreme waves (Lobeto et al., 2021; Meucci et al., 2020; Morim et al., 2023). Such methods require long and reliable time series of wave conditions (long enough to capture the main modes of the local wave climate variability), which then constitute a reference dataset for the comparison with historical model simulations in order to derive parametrized 'correction formulae'. The historical wave datasets currently available for the French Guiana region are not suitable to be used as references for bias correction. Indeed, ERA5 underestimates the wave variables in the Atlantic Ocean, ESA-CCI satellite data is available at monthly frequency and only provide H_s measurements, and the CANDHIS buoy data cover relatively short periods with multiple gaps. Yet, the current model results provide state-of-the-art wave projections, and the application of bias corrections are advised in future research, as appropriate datasets will become available.

The MFWAM model is forced using projected surface wind fields from ARPEGE-Climat (Chauvin et al., 2020), which considers the RCP8.5 future greenhouse gas emission scenario, and include data through 2080. Recently, new Shared Socio-Economic Pathways (SSP) have been developed (Riahi et al., 2017) and adopted within the *IPCC* 6th *Assessment Report* (AR6) together with CMIP6, a new generation of climate models (Eyring et al., 2016). ARPEGE-Climat is developed from one of the CMIP6 models (Roehrig et al., 2020; Voldoire et al., 2013) and has been specifically adapted to properly resolve the atmospheric circulation over the Atlantic basin (Chauvin et al., 2020). However, while ARPEGE-Climat provides state-of-the-art wind projections for our study area, further applications based on SSP scenarios and extending through 2100 would allow coordinating the approach with existing wave projections, such as COWCLIP.

5. Conclusions

Five-member ensemble simulations of present-day and future (RCP-8.5) wave climate over the Atlantic Ocean at 0.5° resolution are forced with wind fields from a single high-resolution GCM to investigate winter wave climate change offshore of French Guiana. Despite an expected increase in wind speed over the French Guiana region, the future wave projections revealed a decrease in average and extreme wave heights and periods across winter, mostly associated with weaker swells from the North Atlantic. A slight clockwise rotation of the incident waves is also expected. The consistency between our projected changes and the

COWCLIP multi-model predictions for the French Guiana region strengthens the confidence in the wave projections presented here. The simulated changes in mean winter wave properties are similar to the ones resulting from existing projections for the summer season, and may contribute to changes in coastal morphodynamics for the French Guiana coast, particularly mud bank dynamics. The comparison between modelled wave climate and the available data highlighted the need for the acquisition of long time series of wave conditions offshore of French Guiana, in order to better assess model skill and correct possible systematic model biases.

Our winter wave projections may have significant implications for the prediction of French Guiana's coastal evolution and flood hazard. We highlight the importance of accounting not only for sea-level rise but also for future wave climate change.

Funding

This work was supported by the Direction Générale des Territoires et de la Mer (DGTM), the Agence Française de Développement (AFD), the Agence de l'Environnement et de la Maîtrise de l'Energie (ADEME), the Office de l'Eau de Guyane (OEG), Météo France and BRGM.

CRediT authorship contribution statement

Maurizio D'Anna: Writing – original draft, Investigation, Formal analysis, Conceptualization. **Léopold Vedie:** Visualization, Software, Investigation, Formal analysis. **Ali Belmadani:** Writing – review & editing, Supervision, Methodology, Formal analysis, Conceptualization. **Déborah Idier:** Writing – review & editing, Conceptualization. **Remi Thiéblemont:** Writing – review & editing, Formal analysis. **Philippe Palany:** Project administration, Funding acquisition. **François Longueville:** Writing – review & editing, Project administration, Funding acquisition.

Declaration of competing interest

The authors declare the following financial interests/personal relationships which may be considered as potential competing interests:

F. Longueville, P. Palany reports financial support was provided by Direction Générale des Territoires et de la Mer. F. Longueville, P. Palany reports financial support was provided by Agence Française de Développement. F. Longueville, P. Palany reports financial support was provided by Agence de l'Environnement et de la Maîtrise de l'Energie. F. Longueville, P. Palany reports financial support was provided by Office de l Eau de Guyane. If there are other authors, they declare that they have no known competing financial interests or personal relationships that could have appeared to influence the work reported in this paper.

Acknowledgements

This study uses altimeter wave data from the ESA-CCI Sea State Project (https://climate.esa.int/en/projects/sea-state/), ERA5 reanalysis wave data produced by the European Centre for Medium-Range Weather Forecasts and distributed by Copernicus (https://cds.climate.copernicus.eu/cdsapp#!/dataset/reanalysis-era5-single-levels?tab=form), and CANDHIS wave buoy data (https://candhis.cerema.fr/_public_/cartes.php). The authors thank F. Chauvin for providing the ARPEGE-Climat model results produced within the C3AF (Changement Climatique et Conséquences sur les Antilles Françaises) project; the COWCLIP contributors for providing freely available multi-model global wave projections; G. Le Cozannet for early discussions; and the anonymous reviewers for the comments. MFWAM model data available upon request.

Supplementary materials

Supplementary material associated with this article can be found, in the online version, at doi:10.1016/j.ocemod.2024.102468.

References

Abascal-Zorrilla, Noelia, Vantrepotte, Vincent, Gensac, Erwan, Huybrechts, Nicolas, Gardel, Antoine, 2018. The advantages of landsat 8-OLI-derived suspended particulate matter maps for monitoring the subtidal extension of amazonian coastal mud banks (French Guiana). Remote Sens. 10 (11), 1–17. https://doi.org/10.3390/rs10111733.

Abascal-Zorrilla, Noelia, Vantrepotte, Vincent, Huybrechts, Nicolas, Ngoc, Dat Dinh, Anthony, Edward J., Gardel, Antoine, 2020. Dynamics of the estuarine turbidity maximum zone from landsat-8 data: the case of the Maroni River Estuary, French Guiana. Remote Sens. 12 (13), 2173. https://doi.org/10.3390/rs12132173.

Aertgeerts, Geoffrey, Longueville, François, 2018. Recensement Et Examen Des Aléaslittoraux Guyanais Entre 1993 Et 2015. Cayenne.

Anthony, Edward J., Gardel, Antoine, Gratiot, Nicolas, Proisy, Christophe, Allison, Mead A., Dolique, Franck, Fromard, François, 2010. The amazon-influenced muddy coast of South America: a review of mud-bank–shoreline interactions. Earth Sci. Rev. 103 (3–4), 99–121. https://doi.org/10.1016/j.earscirev.2010.09.008.

Anthony, E.J., Dolique, F., Gardel, A., Marin, D., 2011. Contrasting Sand beach morphodynamics in a mud-dominated setting: cayenne, French Guiana. J. Coastal Res. 30–34. http://www.jstor.org/stable/26482127.

Ardhuin, F.Abrice, Rick Rogers, E., Babanin, Aexander V, Filipot, Jean Francois, Magne, Rudy, Roland, Aaron, van der Westhuysen, Andre, Queffeulou, Pierre, Lefevre, Jean-Michel, Aouf, Lotfi, Collard, Fabrice, 2010. Semiempirical dissipation source functions for ocean waves. part I : definition, calibration, and validation. J. Phys. Oceanogr. 40 (9), 1917–1941. https://doi.org/10.1175/2010JPO4324.1.

Belmadani, Ali, Dalphinet, Alice, Chauvin, Fabrice, Pilon, Romain, Palany, Philippe, 2021. Projected future changes in tropical cyclone related wave climate in the North Atlantic. Clim. Dyn. 56 (11), 3687–3708. https://doi.org/10.1007/s00382-021-05664-5.

Benjamini, Yoav, Hochberg, Yosef, 1995. Controlling the false discovery rate: a practical and powerful approach to multiple testing. J. R. Stat Soc. Series. B Stat Methodol. 57 (1), 289–300. https://doi.org/10.1111/j.2517-6161.1995.tb02031.x.

Bernardino, M., Gonçalves, M., Soares, C.Guedes, 2021. Marine climate projections toward the end of the twenty-first century in the North Atlantic. J. Offshore Mech. Arct. Eng. 143 (6). https://doi.org/10.1115/1.4050698.

Bidlot, J.R., 2017. Twenty-one years of wave forecast verification. ECMWF Newsletter 150, 31–36.

Bitner-Gregersen, Elzbieta M., Waseda, Takuji, Parunov, Josko, Yim, Solomon, Hirdaris, Spyros, Ma, Ning, Guedes Soares, C., 2022. Uncertainties in long-term wave modelling. Mar. struct. 84, 103217. https://doi.org/10.1016/j.marstruc.2022.103217.

Bricheno, Lucy M., Wolf, Judith, 2018. Future wave conditions of Europe, in response to high-end climate change scenarios. J. Geophys. Res.: Oceans 123 (12), 8762–8791. https://doi.org/10.1029/2018JC013866.

Camus, P., Losada, I.J., Izaguirre, C., Espejo, A., Menéndez, M., Pérez, J., 2017. Statistical wave climate projections for coastal impact assessments. Earth's Futur. 5 (9), 918–933. https://doi.org/10.1002/2017EF000609.

Cantet, Philippe, Belmadani, Ali, Chauvin, Fabrice, Palany, Philippe, 2021. Projections of tropical cyclone rainfall over land with an eulerian approach: case study of three islands in the West Indies. Int. J. Climatol. 41 (S1). https://doi.org/10.1002/joc.6760.

Casas-Prat, M., Wang, X.L., Swart, N., 2018. CMIP5-based global wave climate projections including the entire arctic ocean. Ocean Modell. 123 (November 2017), 66–85. https://doi.org/10.1016/j.ocemod.2017.12.003.

Casas-Prat, Mercè, Hemer, Mark A., Dodet, Guillaume, Morim, Joao, Wang, Xiaolan L., Mori, Nobuhito, Young, Ian, Erikson, Li, Kamranzad, Bahareh, Kumar, Prashant, Menéndez, Melisa, Feng, Yang, 2024. Wind-wave climate changes and their impacts. Nat. Rev. Microbiol. 5 (1), 23–42. https://doi.org/10.1038/s43017-023-00502-0.

Charles, Elodie, Idier, Déborah, Delecluse, Pascale, Déqué, Michel, Cozannet, Gonéri Le, 2012. Climate change impact on waves in the bay of biscay, France. Ocean Dyn. 62 (6). https://doi.org/10.1007/s10236-012-0534-8.

Chauvin, Fabrice, Pilon, Romain, Palany, Philippe, Belmadani, Ali, 2020. Future changes in atlantic hurricanes with the rotated-stretched ARPEGE-climat at very high resolution. Clim. Dyn. 54 (1–2), 947–972. https://doi.org/10.1007/s00382-019-05040-4.

Collins, Jennifer M., Roache, David R., 2017. The 2016 North Atlantic hurricane season: a season of extremes. Geophys. Res. Lett. 44 (10), 5071–5077. https://doi.org/10.1002/2017GL073390.

Cooley, S., Schoeman, D., Bopp, L., Boyd, P., Donner, S., i. Ito, S., Kiessling, W., Martinetto, P., Ojea, E., Racault, M.F., Rost, B., Skern-Mauritzen, M., Ghebrehiwet, D.Y., Bell, J.D., Blanchard, J., Bolin, J., Cheung, W.W., Cisneros-Montemayor, A., Dupont, S., Dutkiewicz, S., Frölicher, T., Gaitán-Espitia, J.D., Molinos, J.G., Gurney-Smith, H., Henson, S., Hidalgo, M., Holland, E., Kopp, R., Kordas, R., Kwiatkowski, L., Le Bris, N., Lluch-Cota, S.E., Logan, C., Mark, F.C., Mgaya, Y., Moloney, C., Muñoz Sevilla, N.P., Randin, G., Raja, N.B., Rajkaran, A., Richardson, A., Roe, S., Ruiz Diaz, R., Salili, D., Sallée, J.B., Scales, K., Scobie, M., Simmons, C.T., Torres, O., Yool, A., 2022. Oceans and coastal ecosystems and their services. In: Climate Change 2022: Impacts, adaptation and vulnerability. Contribution of the WGII to the 6th assessment report of the intergovernmental

panel on climate change. IPCC AR6 WGII. Cambridge University Press edited by. https://www.ipcc.ch/report/ar6/wg2/downloads/report/IPCC_AR6_WGII_FinalDraft_Chapter03.pdf.

D'Agostini, Andressa, Bernardino, Mariana, Guedes Soares, C., 2022. Projected wave storm conditions under the RCP8.5 climate change scenario in the North Atlantic Ocean. Ocean Eng. 266 (P3), 112874. https://doi.org/10.1016/j.oceaneng.2022.112874.

D'Anna, Maurizio, Idier, Déborah, Castelle, Bruno, Rohmer, Jérémy, Cagigal, Laura, Mendez, Fernando J., 2022. Effects of stochastic wave forcing on probabilistic equilibrium shoreline response across the 21st century including sea-level rise. Coastal Eng. 175 (May), 104149. https://doi.org/10.1016/j.coastaleng.2022.104149.

Déqué, Michel., 2007. Frequency of precipitation and temperature extremes over france in an anthropogenic scenario: model results and statistical correction according to observed values. Global Planet. Change 57, 16–26.

Dodet, Guillaume, Piolle, Jean-François, Quilfen, Yves, Abdalla, Saleh, Accensi, Mickaël, Ardhuin, Fabrice, Ash, Ellis, Bidlot, Jean-Raymond, Gommenginger, Christine, Marechal, Gwendal, Passaro, Marcello, Quartly, Graham, Stopa, Justin, Timmermans, Ben, Young, Ian, Cipollini, Paolo, Donlon, Craig, 2020. The sea state CCI dataset v1: towards a sea state climate data record based on satellite observations. Earth Syst. Sci. Data 12 (3), 1929–1951. https://doi.org/10.5194/essd-12-1929-2020.

Eisma, D., Augustinus, P.G.E.F., Alexander, C., 1991. Recent and subrecent changes in the dispersal of amazon mud. Neth. J. Sea Res. 28 (3), 181–192. https://doi.org/10.1016/0077-7579(91)90016-T.

Erikson, L., Morim, J., Hemer, M., Young, I., Wang, X.L., Mentaschi, L., Mori, N., Semedo, A., Stopa, J., Grigorieva, V., Gulev, S., Aarnes, O., Bidlot, J.R., Breivik, Ø., Bricheno, L., Shimura, T., Menendez, M., Markina, M., Sharmar, V., Trenham, C., Wolf, J., Appendini, C., Caires, S., Groll, N., Webb, A., 2022. Global Ocean wave fields show consistent regional trends between 1980 and 2014 in a multi-product ensemble. Commun. Earth Environ. 3 (1), 320. https://doi.org/10.1038/s43247-022-00654-9.

Eyring, Veronika, Bony, Sandrine, Meehl, Gerald A., Senior, Catherine A., Stevens, Bjorn, Stouffer, Ronald J., Taylor, Karl E., 2016. Overview of the coupled model intercomparison project phase 6 (CMIP6) experimental design and organization. Geosci. Model Dev. 9 (5), 1937–1958. https://doi.org/10.5194/gmd-9-1937-2016.

Fan, Yalin, Held, Isaac M., Lin, Shian-Jiann, Wang, Xiaolan L., 2013. Ocean warming effect on surface gravity wave climate change for the end of the twenty-first century. J. Clim. 26 (16), 6046–6066. https://doi.org/10.1175/JCLI-D-12-00410.1.

Fan, Yalin, Lin, Shian-Jiann, Griffies, Stephen M., Hemer, Mark A., 2014. Simulated global swell and wind-sea climate and their responses to anthropogenic climate change at the end of the twenty-first century. J. Clim. 27 (10), 3516–3536. https://doi.org/10.1175/JCLI-D-13-00198.1.

Froidefond, J.M., Pujos, M., Andre, X., 1988. Migration of mud banks and changing coastline in French Guiana. Mar. Geol. 84 (1–2), 19–30. https://doi.org/10.1016/0025-3227(88)90122-3.

Gardel, Antoine, Gratiot, Nicolas, 2005. A satellite image-based method for estimating rates of mud bank migration, French Guiana, South America. J. Coastal Res. 21 (4), 720–728. https://doi.org/10.2112/03-0100.1.

Gensac, E., Lesourd, S., Gardel, A., Anthony, E.J., Proisy, C., Loisel, H., 2011. Short-term prediction of the evolution of mangrove surface areas: the example of the mud banks of Kourou and Sinnamary, French Guiana. J. Coastal Res. (SPEC ISSUE 64), 388–392.

Gensac, Erwan, Gardel, Antoine, Lesourd, Sandric, Brutier, Laurent, 2015. Morphodynamic evolution of an intertidal mudflat under the influence of amazon sediment supply – kourou mud bank, French Guiana, South America. Estuarine Coastal Shelf Sci. 158, 53–62. https://doi.org/10.1016/j.ecss.2015.03.017.

Gratiot, Nicolas, Gardel, Antoine, Anthony, Edward J., 2007. Trade-wind waves and mud dynamics on the French Guiana Coast, South America: input from ERA-40 wave data and field investigations. Mar. Geol. 236 (1–2), 15–26. https://doi.org/10.1016/j.margeo.2006.09.013.

Hawkins, Timothy W., Gouirand, Isabelle, Allen, Theodore, Belmadani, Ali, 2022. Atmospheric drivers of Oceanic North Swells in the Eastern Caribbean. J. Mar. Sci. Eng. 10 (2), 183. https://doi.org/10.3390/jmse10020183.

Hemer, Mark A., Fan, Yalin, Mori, Nobuhito, Semedo, Alvaro, Wang, Xiaolan L., 2013a. Projected changes in wave climate from a multi-model ensemble. Nat. Clim. Change 3 (5), 471–476. https://doi.org/10.1038/nclimate1791.

Hemer, Mark A., Katzfey, Jack, Trenham, Claire E., 2013b. Global Dynamical projections of surface ocean wave climate for a future high greenhouse gas emission scenario. Ocean Modell. 70, 221–245. https://doi.org/10.1016/j.ocemod.2012.09.008.

Hemer, Mark A., X. Wang, A. Webb, and COWCLIP. 2018. *Report of the 2018 meeting for the WCRP-JCOMM Coordinated global wave climate projections.*

Hersbach, Hans, Bell, Bill, Berrisford, Paul, Hirahara, Shoji, Horányi, András, Muñoz-Sabater, Joaquín, Nicolas, Julien, Peubey, Carole, Radu, Raluca, Schepers, Dinand, Simmons, Adrian, Soci, Cornel, Abdalla, Saleh, Abellan, Xavier, Balsamo, Gianpaolo, Bechtold, Peter, Biavati, Gionata, Bidlot, Jean, Bonavita, Massimo, Chiara, Giovanna, Dahlgren, Per, Dee, Dick, Diamantakis, Michail, Dragani, Rossana, Flemming, Johannes, Forbes, Richard, Fuentes, Manuel, Geer, Alan, Haimberger, Leo, Healy, Sean, Hogan, Robin J., Hólm, Elías, Janisková, Marta, Keeley, Sarah, Laloyaux, Patrick, Lopez, Philippe, Lupu, Cristina, Radnoti, Gabor, Rosnay, Patricia, Rozum, Iryna, Vamborg, Freja, Villaume, Sebastien, Thépaut, Jean-Noël, 2020. The ERA5 Global Reanalysis. Q. J. R. Meteorolog. Soc. 146 (730), 1999–2049. https://doi.org/10.1002/qj.3803.

Hinkel, Jochen, Church, John A., Gregory, Jonathan M., Lambert, Erwin, Cozannet, Gonéri Le, Lowe, Jason, McInnes, Kathleen L., Nicholls, Robert J., Pol, Thomas D., Wal, Roderik, 2019. Meeting user needs for sea level rise information: a decision analysis perspective. Earth's Futur. 7 (3), 320–337. https://doi.org/10.1029/2018EF001071.

Hinkel, J., Feyen, L., Hemer, Mark A., Cozannet, G.Le, Lincke, D., Marcos, M., Mentaschi, L., Merkens, J.L., de Moel, H., Muis, S., Nicholls, R.J., Vafeidis, A.T., van de Wal, R.S.W., Vousdoukas, M.I., Wahl, T., Ward, P.J., Wolff, C., 2021. Uncertainty and bias in global to regional scale assessments of current and future coastal flood risk. Earth's Futur. 9 (7). https://doi.org/10.1029/2020EF001882.

Jolivet, Morgane, Gardel, Antoine, Anthony, Edward J., 2019. Multi-decadal changes on the mud-dominated coast of Western French Guiana: implications for mesoscale shoreline mobility, river-mouth deflection, and sediment sorting. J. Coastal Res. 88 (sp1), 185. https://doi.org/10.2112/SI88-014.1.

Jolivet, Morgane, Anthony, Edward J., Gardel, Antoine, Maury, Tanguy, Morvan, Sylvain, 2022. Dynamics of mud banks and sandy urban beaches in French Guiana, South America. Reg. Environ. Change 22 (3), 101. https://doi.org/10.1007/s10113-022-01944-w.

Khandekar, M.L., 1989. Validation of wave models. Operational Analysis and Prediction of Ocean Wind Waves. Springer New York, New York, NY, pp. 127–164.

Kodaira, Tsubasa, Sasmal, Kaushik, Miratsu, Rei, Fukui, Tsutomu, Zhu, Tingyao, Waseda, Takuji, 2023. Uncertainty in wave hindcasts in the North Atlantic Ocean. Mar. Struct. 89, 103370. https://doi.org/10.1016/j.marstruc.2023.103370.

Lakhan, V.Chris, Pepper, David A., 1997. Relationship between concavity and convexity of a coast and erosion and accretion patterns. J. Coastal Res. 13 (1), 226–232. https://www.jstor.org/stable/4298609.

Le Cozannet, Gonéri, Idier, Déborah, de Michele, Marcello, Legendre, Yoann, Moisan, Manuel, Pedreros, Rodrigo, Thiéblemont, Rémi, Spada, Giorgio, Raucoules, Daniel, de la Torre, Ywenn, 2021. Timescales of emergence of chronic flooding in the major economic center of guadeloupe. Nat. Hazards Earth Syst. Sci. 21 (2), 703–722. https://doi.org/10.5194/nhess-21-703-2021.

Lemos, Gil, Semedo, Alvaro, Dobrynin, Mikhail, Behrens, Arno, Staneva, Joanna, Bidlot, Jean-Raymond, Miranda, Pedro M.A., 2019. Mid-twenty-first century global wave climate projections: results from a dynamic CMIP5 based ensemble. Global Planet. Change 172, 69–87. https://doi.org/10.1016/j.gloplacha.2018.09.011.

Lemos, Gil, Menendez, Melisa, Semedo, Alvaro, Camus, Paula, Hemer, Mark A., Dobrynin, Mikhail, Miranda, Pedro M.A., 2020. On the need of bias correction methods for wave climate projections. Global Planet. Change 186, 103109. https://doi.org/10.1016/j.gloplacha.2019.103109.

Lemos, Gil, Menendez, Melisa, Semedo, Alvaro, Miranda, Pedro M.A., Hemer, Mark A., 2021. On the decreases in North Atlantic significant wave heights from climate projections. Clim. Dyn. 57 (9), 2301–2324. https://doi.org/10.1007/s00382-021-05807-8.

Lemos, Gil, Bosnic, Ivana, Antunes, Carlos, Vousdoukas, Michalis, Mentaschi, Lorenzo, Santo, Miguel Espírito, Ferreira, Vanessa, Soares, Pedro M.M., 2024. The future of the portuguese (SW Europe) most vulnerable coastal areas under climate change – part II: future Extreme coastal flooding from downscaled bias corrected wave climate projections. Ocean Eng. 310, 118448. https://doi.org/10.1016/j.oceaneng.2024.118448.

Lira Loarca, Andrea, Berg, Peter, Baquerizo, Asuncion, Besio, Giovanni, 2023. On the role of wave climate temporal variability in bias correction of wave climate projections. Clim. Dyn. https://doi.org/10.21203/rs.3.rs-1986616/v1.

Lobeto, Hector, Menendez, Melisa, Losada, Iñigo J., 2021. Future behavior of wind wave extremes due to climate change. Sci. Rep. 11 (1), 7869. https://doi.org/10.1038/s41598-021-86524-4.

Lobeto, Hector, Menendez, Melisa, Losada, Iñigo J., Hemer, Mark A., 2022. The effect of climate change on wind-wave directional spectra. Global Planet. Change 213, 103820. https://doi.org/10.1016/j.gloplacha.2022.103820.

Longueville, François, Lanson, Méline, 2022. Épisodes D'érosion Du 3 Au 7 Janvier 2022 Sur Le Littoral d'Awala-Yalimapo (Guyane) : Avis et Recommandations Du BRGM. Cayenne.

Longueville, François, Rémi Thiéblemont, Ali Belmadani, Déborah Idier, Philippe Palany, Maurizio D'Anna, Pierre-Christian Dutrieux, Léopold Védie, Méline Lanson, and Baptiste Suez-Panama-Bouton. 2022. *Impacts Du Changement Climatique Sur Différents Paramètres Physiques En Guyane : caractérisation et Projection - GuyaClimat.*

Longueville, François., 2017. Rapport d'expertise: Observations Suite Aux Épisodes D'érosion Marine de Fin d'année 2016 Sur Le Littoral de Kourou (Guyane). Cayenne.

Mankin, Justin S., Lehner, Flavio, Coats, Sloan, McKinnon, Karen A., 2020. The value of initial condition large ensembles to robust adaptation decision-making. Earth's Futur. 8 (10). https://doi.org/10.1029/2020EF001610.

Meucci, Alberto, Young, Ian R., Hemer, Mark A., Kirezci, Ebru, Ranasinghe, Roshanka, 2020. Projected 21st century changes in extreme wind-wave events. Sci. Adv. 6 (24). https://doi.org/10.1126/sciadv.aaz7295.

Meucci, Alberto, Young, Ian R., Hemer, Mark, Trenham, Claire, Watterson, Ian G., 2023. 140 Years of global ocean wind-wave climate derived from CMIP6 ACCESS-CM2 and EC-Earth3 GCMs: global trends, regional changes, and future projections. J. Clim. 36 (6), 1605–1631. https://doi.org/10.1175/JCLI-D-21-0929.1.

Meucci, Alberto, Young, Ian R., Trenham, Claire, Hemer, Mark, 2024. An 8-model ensemble of CMIP6-derived ocean surface wave climate. Sci Data 11 (1), 100. https://doi.org/10.1038/s41597-024-02932-x.

Mori, Nobuhito, Tomohiro Yasuda, Hajime Mase, Tracey Tom, and Yuichiro Oku. 2010. "Projection of extreme wave climate change under global warming." 19:15–19. doi: 10.3178/HRL.4.15.

Mori, Nobuhito, Shimura, Tomoya, Yasuda, Tomohiro, Mase, Hajime, 2013. Multi-model climate projections of ocean surface variables under different climate scenarios—future change of waves, sea level and wind. Ocean Eng. 71, 122–129. https://doi.org/10.1016/j.oceaneng.2013.02.016.

Morim, Joao, Hemer, Mark, Wang, Xiaolan L., Cartwright, Nick, Trenham, Claire, Semedo, Alvaro, Young, Ian, Bricheno, Lucy, Camus, Paula, Casas-Prat, Mercè,

Erikson, Li, Mentaschi, Lorenzo, Mori, Nobuhito, Shimura, Tomoya, Timmermans, Ben, Aarnes, Ole, Breivik, Øyvind, Behrens, Arno, Dobrynin, Mikhail, Menendez, Melisa, Staneva, Joanna, Wehner, Michael, Wolf, Judith, Kamranzad, Bahareh, Webb, Adrean, Stopa, Justin, Andutta, Fernando, 2019. Robustness and uncertainties in global multivariate wind-wave climate projections. Nat. Clim. Change 9 (9). https://doi.org/10.1038/s41558-019-0542-5.

Morim, Joao, Trenham, Claire, Hemer, Mark, Wang, Xiaolan L., Mori, Nobuhito, Casas-Prat, Mercè, Semedo, Alvaro, Shimura, Tomoya, Timmermans, Ben, Camus, Paula, Bricheno, Lucy, Mentaschi, Lorenzo, Dobrynin, Mikhail, Feng, Yang, Erikson, Li, 2020. A global ensemble of ocean wave climate projections from CMIP5-driven models. Sci. Data 7 (1), 105. https://doi.org/10.1038/s41597-020-0446-2.

Morim, J., Erikson, L.H., Hemer, M., Young, I., Wang, X., Mori, N., Shimura, T., Stopa, J., Trenham, C., Mentaschi, L., Gulev, S., Sharmar, V.D., Bricheno, L., Wolf, J., Aarnes, O., Perez, J., Bidlot, J., Semedo, A., Reguero, B., Wahl, T., 2022. A global ensemble of ocean wave climate statistics from contemporary wave reanalysis and hindcasts. Sci Data 9 (1), 358. https://doi.org/10.1038/s41597-022-01459-3.

Morim, Joao, Wahl, Thomas, Vitousek, Sean, Santamaria-Aguilar, Sara, Young, Ian R., Hemer, Mark A., 2023. Understanding uncertainties in contemporary and future extreme wave events for broad-scale impact and adaptation planning. Sci. Adv. 9 (2). https://doi.org/10.1126/sciadv.ade3170.

Parodi, Matteo U., Giardino, Alessio, Dongeren, Ap van, Pearson, Stuart G., Bricker, Jeremy D., Reniers, Ad J.H.M., 2020. Uncertainties in coastal flood risk assessments in small island developing states. Nat. Hazards Earth Syst. Sci. 20 (9), 2397–2414. https://doi.org/10.5194/nhess-20-2397-2020.

Piollé, J.F., G. Dodet, Y. Quilfen, and ESA Sea State Climate Change Initiative. 2020. *Global remote sensing merged multi-mission monthly gridded significant wave height, L4 product, version 1.1*.

Rayner, N.A., 2003. Global analyses of sea surface temperature, sea ice, and night marine air temperature since the late nineteenth century. J. Geophys. Res. 108 (D14), 4407. https://doi.org/10.1029/2002JD002670.

Reguero, Borja G., Losada, Iñigo J., Méndez, Fernando J., 2019. A recent increase in global wave power as a consequence of oceanic warming. Nat. Commun. 10 (1), 205. https://doi.org/10.1038/s41467-018-08066-0.

Riahi, Keywan, Vuuren, Detlef P.van, Kriegler, Elmar, Edmonds, Jae, O'Neill, Brian C., Fujimori, Shinichiro, Bauer, Nico, Calvin, Katherine, Dellink, Rob, Fricko, Oliver, Lutz, Wolfgang, Popp, Alexander, Cuaresma, Jesus Crespo, Samir, K.C., Leimbach, Marian, Jiang, Leiwen, Kram, Tom, Rao, Shilpa, Emmerling, Johannes, Ebi, Kristie, Hasegawa, Tomoko, Havlik, Petr, Humpenöder, Florian, Silva, Lara Aleluia Da, Smith, Steve, Stehfest, Elke, Bosetti, Valentina, Eom, Jiyong, Gernaat, David, Masui, Toshihiko, Rogelj, Joeri, Strefler, Jessica, Drouet, Laurent, Krey, Volker, Luderer, Gunnar, Harmsen, Mathijs, Takahashi, Kiyoshi, Baumstark, Lavinia, Doelman, Jonathan C., Kainuma, Mikiko, Klimont, Zbigniew, Marangoni, Giacomo, Lotze-Campen, Hermann, Obersteiner, Michael, Tabeau, Andrzej, Tavoni, Massimo, 2017. The shared socioeconomic pathways and their energy, land use, and greenhouse gas emissions implications: an overview. Glob. Environ. Chang. 42, 153–168. https://doi.org/10.1016/j.gloenvcha.2016.05.009.

Roehrig, Romain, Beau, Isabelle, Saint-Martin, David, Alias, Antoinette, Decharme, Bertrand, Guérémy, Jean-François, Voldoire, Aurore, Younous Abdel-Lathif, Ahmat, Bazile, Eric, Belamari, Sophie, Blein, Sebastien, Bouniol, Dominique, Bouteloup, Yves, Cattiaux, Julien, Chauvin, Fabrice, Chevallier, Matthieu, Colin, Jeanne, Douville, Hervé, Marquet, Pascal, Michou, Martine, Nabat, Pierre, Oudar, Thomas, Peyrillé, Philippe, Piriou, Jean-Marcel, Salas y Mélia, David, Séférian, Roland, Sénési, Stéphane, 2020. The CNRM global atmosphere model ARPEGE-climat 6.3: description and evaluation. J. Adv. Model Earth Syst. 12 (7). https://doi.org/10.1029/2020MS002075.

Semedo, Alvaro, Weisse, Ralf, Behrens, Arno, Sterl, Andreas, Bengtsson, Lennart, Günther, Heinz, 2012. Projection of global wave climate change toward the end of the twenty-first century. J. Clim. 26 (21), 8269–8288. https://doi.org/10.1175/JCLI-D-12-00658.1.

Semedo, Alvaro, Weisse, Ralf, Behrens, Aarno, Sterl, Andreas, Bengtsson, Lennart, Gunther, Heinz, 2013. Projection of global wave climate change toward the end of the twenty-first century. J. Clim. 26 (21), 8269–8288. https://doi.org/10.1175/JCLI-D-12-00658.1.

Semedo, Alvaro, Dobrynin, Mikhail, Lemos, Gil, Behrens, Arno, Staneva, Joanna, de Vries, Hylke, Sterl, Andreas, Bidlot, Jean-Raymond, Miranda, Pedro, Murawski, Jens, 2018. CMIP5-derived single-forcing, single-model, and single-scenario wind-wave climate ensemble: configuration and performance evaluation. J. Mar. Sci. Eng. 6 (3), 90. https://doi.org/10.3390/jmse6030090.

Thiéblemont, Remi, Le Cozannet Goneri, Maurizio, D'Anna, Idier, Déborah, Belmadani, Ali, Slangen, Aimée, Longueville, François, 2023. Chronic flooding events due to sea-level rise in French Guiana. Sci. Rep. 13, 21695. https://doi.org/10.1038/s41598-023-48807-w.

Timmermans, Ben, Stone, Dáithí, Wehner, Michael, Krishnan, Harinarayan, 2017. Impact of tropical cyclones on modeled extreme wind-wave climate. Geophys. Res. Lett. 44 (3), 1393–1401. https://doi.org/10.1002/2016GL071681.

Timmermans, Ben, Gommenginger, C.P., Dodet, G., Bidlot, J.-R., 2020. Global wave height trends and variability from new multimission satellite altimeter products, reanalyses, and wave buoys. Geophys. Res. Lett. 47 (9). https://doi.org/10.1029/2019GL086880.

Toimil, Alexandra, Camus, Paula, Losada, Iñigo J., Cozannet, Gonéri Le, Nicholls, Robert J., Idier, Déborah, Maspataud, Aurelie, 2020. Climate change-driven coastal erosion modelling in temperate sandy beaches: methods and uncertainty treatment. Earth Sci. Rev. 202. https://doi.org/10.1016/j.earscirev.2020.103110.

Toimil, Alexandra, Camus, Paula, Losada, Iñigo J., Alvarez-Cuesta, Moises, 2021. Visualising the uncertainty cascade in multi-ensemble probabilistic coastal erosion projections. Front. Mar. Sci. 8. https://doi.org/10.3389/fmars.2021.683535.

Vantrepotte, V., Gensac, E., Loisel, H., Gardel, A., Dessailly, D., Mériaux, X., 2013. Satellite assessment of the coupling between in water suspended particulate matter and mud banks dynamics over the French Guiana coastal domain. J. South Amer. Earth Sci. 44, 25–34. https://doi.org/10.1016/j.jsames.2012.11.008.

Voldoire, A., Sanchez-Gomez, E., Salas y Mélia, D., Decharme, B., Cassou, C., Sénési, S., Valcke, S., Beau, I., Alias, A., Chevallier, M., Déqué, M., Deshayes, J., Douville, H., Fernandez, E., Madec, G., Maisonnave, E., Moine, M.P., Planton, S., Saint-Martin, D., Szopa, S., Tyteca, S., Alkama, R., Belamari, S., Braun, A., Coquart, L., Chauvin, F., 2013. The CNRM-CM5.1 global climate model: description and basic evaluation. Clim. Dyn. 40 (9–10), 2091–2121. https://doi.org/10.1007/s00382-011-1259-y.

Voldoire, A., Saint-Martin, D., Sénési, S., Decharme, B., Alias, A., Chevallier, M., Colin, J., Guérémy, J.-F., Michou, M., Moine, M.-P., Nabat, P., Roehrig, R., Salas y Mélia, D., Séférian, R., Valcke, S., Beau, I., Belamari, S., Berthet, S., Cassou, C., Cattiaux, J., Deshayes, J., Douville, H., Ethé, C., Franchistéguy, L., Geoffroy, O., Lévy, C., Madec, G., Meurdesoif, Y., Msadek, R., Ribes, A., Sanchez-Gomez, E., Terray, L., Waldman, R., 2019. Evaluation of CMIP6 DECK experiments With CNRM-CM6-1. J. Adv. Model Earth Syst. 11 (7), 2177–2213. https://doi.org/10.1029/2019MS001683.

Vousdoukas, Michalis I., Bouziotas, Dimitrios, Giardino, Alessio, Bouwer, Laurens M., Mentaschi, Lorenzo, Voukouvalas, Evangelos, Feyen, Luc, 2018. Understanding epistemic uncertainty in large-scale coastal flood risk assessment for present and future climates. Nat. Hazards Earth Syst. Sci. 18 (8), 2127–2142. https://doi.org/10.5194/nhess-18-2127-2018.

WAMDI-Group, 1988. The WAM model: a third-generation ocean wave prediction model. J. Phys. Oceanogr. 18, 1775–1810.

Wang, Xiaolan L., Feng, Yang, Swail, Val R., 2014. Changes in global ocean wave heights as projected using multimodel CMIP5 simulations. Geophys. Res. Lett. 41 (3), 1026–1034. https://doi.org/10.1002/2013GL058650.

Webb, Adrean, Shimura, Tomoya, Mori, Nobuhito, 2018. A high-resolution future wave climate projection for the coastal Northwestern Atlantic. J. Japan Soc. Civil Eng. Ser. B2 (Coastal Eng.) 74 (2), 1345–1350. https://doi.org/10.2208/kaigan.74.I_1345.

Wells, John T., and G.Paul Kemp. 1986. "Interaction of surface waves and cohesive sediments: field observations and geologic significance." pp. 43–65 in *Lecture Notes on Coastal and Estuarine Studies*, edited by A. J. Mehta.

Yadav, Anshu, Kumar, Prashant, Bhaskaran, Prasad Kumar, Hisaki, Yukiharu, Rajni, 2024. Evaluation of ocean wave power utilizing COWCLIP 2.0 Datasets: a CMIP5 model assessment. Clim. Dyn. https://doi.org/10.1007/s00382-024-07402-z.

Young, Ian R., 1999. Seasonal variability of the global ocean wind and wave climate. Int. J. Climatol. 19, 931–950. https://doi.org/10.1002/(SICI)1097-0088(199907).